AD-A108 291 STATE UNIV OF NEW YORK AT ALBANY SPACE ASTRONOMY LAB F/G 20/6
EXPERIMENTAL RESULTS OF MULTIPLE SCATTERING.(U)
NOV 81 D W SCHUERMAN, R T WANG DAAG29-79-C-0055
UNCLASSIFIED ARCSL-CR-81003 NL

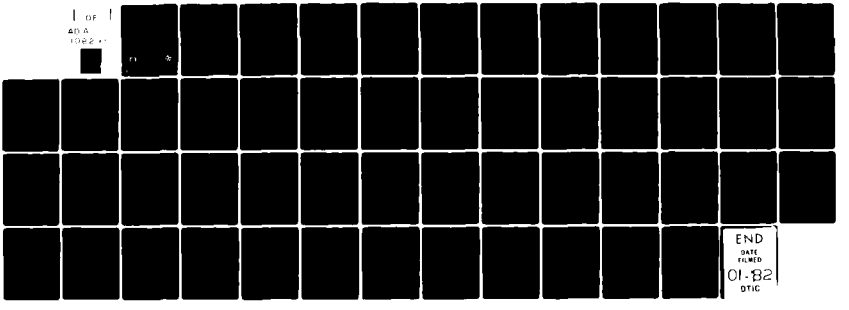

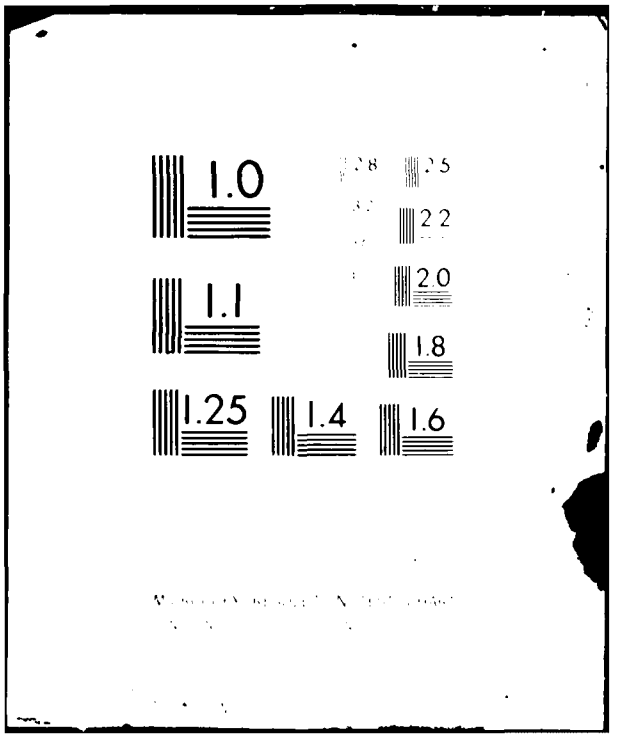
1.0
1.1
1.25
1.4
1.6
1.8
2.0
2.2

CHEMICAL SYSTEMS LABORATORY CONTRACTOR REPORT

ARCSL-CR-81003

EXPERIMENTAL RESULTS OF MULTIPLE SCATTERING

Final Report

by

Donald W. Schuerman
Ru T. Wang

November 1981

STATE UNIVERSITY OF NEW YORK AT ALBANY
Space Astronomy Laboratory
Executive Park East
Albany, New York 12203

Contract DAAG29-79-C-0055

US ARMY ARMAMENT RESEARCH AND DEVELOPMENT COMMAND
Chemical Systems Laboratory
Aberdeen Proving Ground, Maryland 21010

Disclaimer

The views, opinions and/or findings contained in this report are those of the author and should not be construed as an official Department of the Army position, policy, or decision unless so designated by other documentation.

Disposition

Destroy this report when it is no longer needed. Do not return it to the originator.

UNCLASSIFIED

SECURITY CLASSIFICATION OF THIS PAGE (When Data Entered)

REPORT DOCUMENTATION PAGE		READ INSTRUCTIONS BEFORE COMPLETING FORM
1. REPORT NUMBER ARCSL-CR-81003	2. GOVT ACCESSION NO. AD-A108 291	3. RECIPIENT'S CATALOG NUMBER
4. TITLE (and Subtitle) EXPERIMENTAL RESULTS OF MULTIPLE SCATTERING		5. TYPE OF REPORT & PERIOD COVERED Final March 1979 to July 1980 6. PERFORMING ORG. REPORT NUMBER
7. AUTHOR(s) Donald W. Schuerman Ru T. Wang		8. CONTRACT OR GRANT NUMBER(s) DAAG29-79-C-0055
9. PERFORMING ORGANIZATION NAME AND ADDRESS State University of New York at Albany Space Astronomy Laboratory Executive Park East, Albany, New York 12203		10. PROGRAM ELEMENT, PROJECT, TASK AREA & WORK UNIT NUMBERS
11. CONTROLLING OFFICE NAME AND ADDRESS Commander/Director, Chemical Systems Laboratory ATTN: DRDAR-CLJ-R Aberdeen Proving Ground, Maryland 21010		12. REPORT DATE November 1981 13. NUMBER OF PAGES 54
14. MONITORING AGENCY NAME & ADDRESS(if different from Controlling Office) U. S. Army Research Office Post Office Box 12211 Research Triangle Park, NC 27709		15. SECURITY CLASS. (of this report) UNCLASSIFIED 15a. DECLASSIFICATION/DOWNGRADING SCHEDULE NA

16. DISTRIBUTION STATEMENT (of this Report)

Approved for public release; distribution unlimited.

17. DISTRIBUTION STATEMENT (of the abstract entered in Block 20, if different from Report)

18. SUPPLEMENTARY NOTES

Contract Project Officer: Dr. Edward Stuebing (DRDAR-CLB-PS, 301-671-3089)

19. KEY WORDS (Continue on reverse side if necessary and identify by block number)

Light-scattering
Multiple scattering
Dependent light scattering
Extinction

20. ABSTRACT (Continue on reverse side if necessary and identify by block number)

Microwave analog measurements of scattering by ensembles of 2^n(n=1,2,3) interacting spheres are presented. Emphasis is placed on the amplitude and phase measurements of the forward (θ=0°) scattered wave as a function of the mutual separation of the spheres and the orientation of the ensembles with respect to the incident beam. A few side scattering (θ=90°) and angular distribution (40°$\leq\theta\leq$140°) measurements indicate the existence of specular

(Continued on reverse side)

DD FORM 1 JAN 73 1473 EDITION OF 1 NOV 65 IS OBSOLETE

UNCLASSIFIED

SECURITY CLASSIFICATION OF THIS PAGE (When Data Entered)

20. ABSTRACT (Contd)

scattering at particular array orientations for some of the two-sphere ensembles. A short historical sketch, a description of the experiments, and phenomenological explanations of the results are also given.

FOREWORD

In 1958, Dr. J. Mayo Greenberg (now at the University of Leiden, Netherlands) established a microwave analog facility to investigate the extinction of light by small, irregular particles. Joined by Dr. Ru T. Wang in 1960 and later by Dr. Donald W. Schuerman in 1972 (who now directs the facility), the facility has fostered numerous investigations of both the extinction and angular scattering of radiation by particles whose size is of the order of the incident wavelength. Many of these studies have gone unpublished. Under this contract, we have selected a fairly large number of intriguing scattering results, put them in a form appropriate for publication, and tried, where possible, to provide physical interpretations. Our desire is to disseminate the results of these unique measurements. This report is part of that endeavor. Another portion of this study, entitled "Extinction Signatures of Non-Spherical/Non-Isotropic Particles" by Ru T. Wang, appeared in the book LIGHT SCATTERING BY IRREGULARLY SHAPED PARTICLES (Edited by D. W. Schuerman, Plenum Publishing Corp., 1980). An abbreviated or summary version of these two articles will soon be submitted for publication in the journal OPTICS LETTERS. That summary article refers interested readers to this report.

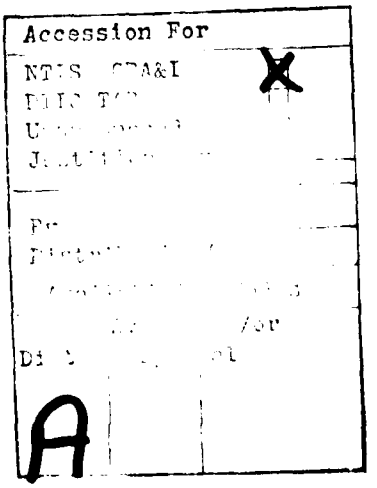

PREFACE

This work is sponsored by the U. S. Army Research Office, under contract DAAG29-79-C-0055. Some of the work was carried out as early as 1968, and this is an account of work from March 1979 to July 1980 on the extinction and angular scattering of radiation by particles of size the order of the incident wavelength.

SUMMARY

Microwave analog measurements of scattering by ensembles of 2^n(n=1,2,3) interacting spheres are presented. Emphasis is placed on the amplitude and phase measurements of the forward ($\theta=0^o$) scattered wave as a function of the mutual separation of the spheres and the orientation of the ensembles with respect to the incident beam. The results are displayed as calibrated P,Q plots; i.e., cartesian displays of the complex amplitude. A short historical sketch, a description of the experiment, and phenomenological explanations of the results are also given. Side scattering ($\theta=90^o$) and angular distribution ($40^o \leq \theta \leq 140^o$) measurements indicate the existence of specular scattering at particular array orientations for some of the two-sphere ensembles.

CONTENTS

EXPERIMENTAL RESULTS OF MUTLIPLE SCATTERING

1. INTRODUCTION

Small particles scatter light quite differently depending on whether they are mutually well separated or in close proximity. This is quite obvious if we consider the two extreme cases of two spheres either far apart or in contact (a single particle). The earliest theoretical investigation of dependently scattering particles seems to be that by Trinks (1935) who formulated the solution of Maxwell's equations for a two-sphere problem of rather small particle size. Despite the mathematical complexity, theoretical work continued (see Germogenova, 1963; Liang and Lo, 1967; Levine and Olaofe, 1968; Rozenberg, 1971; Bruning and Lo, 1969, 1971). In these rigorous solution approaches, one still sums the scattering by individual particles to evaluate the total scattering from the array. To compute the scattering from each sphere, taking into account the near field effect of the neighboring particle requires the rather complex procedure of relocating the spherical vector wave functions from one particle origin to the other to form a proper boundary-value problem. This procedure results in extremely complicated expressions. Although the advent of modern computers and the development of efficient algorithms make the numerical evaluation more accessible (Bruning and Lo, 1971), it is still difficult to obtain a clear physical picture of dependent scattering. We have also to mention the very ingenious, yet complex theoretical works of Twersky (1967), Waterman and Truell (1961) and the less formidable but still difficult works of Hongo (1978), Borghese et al. (1979) and Kattawar and Humphreys (1980). Like those in the single-particle cases (van de Hulst, 1957; Kerker, 1969), the problem of multiple-particle scattering has many stumbling blocks if pursued by theoretical approaches alone. Indeed, even in a static field the problem of finding the induced dipole moment on 2 spheres as a function of mutual separation is already quite involved (Goyette and Navon, 1976).

Experimental investigations on multiple-particle scattering, although scarce, have also been sporadically reported during the past two decades. Perhaps such a study is next to impossible in the optical region (Woodward, 1964), and the few experiments conducted in the microwave region were performed mostly for the backscattering ($\theta=180^{\circ}$). Angelakos and Kumagai (1964) obtained backscatter results for multiple conducting spheres and compared them with the predictions of geometrical optics. To verify their theoretical results, Bruning and Lo (1969, 1971) performed such experiments for both conducting and penetrable multiple spheres. The only exception in which an extinction ($\theta=0^{\circ}$) experiment was performed is by Beard, et al. (1967 and references cited therein) who investigated multiple spheres in random motion, recorded the quadrature phase components of such aggregates, and subsequently compared the results with the statistical theory of Hawley et al. (1967). Disregarding the technical difficulties of using millimeter waves for the $\theta=0^{\circ}$ scattering research, the random particle motion alone may completely obscure the detailed picture of dependent scattering.

Encouraged by the initial success of $\theta=0^{\circ}$ microwave measurements (Lind et al., 1965) for nonspherical particles which permitted us to observe detailed phenomena with precisely known target parameters and orientations, we extended the analog method to cover the dependent-scattering studies by replacing a nonspherical particle with an array of spheres. Some $\theta=90^{\circ}$ and $40^{\circ}\leq\theta\leq140^{\circ}$ scattering measurements were also made to explore

the elegant mathematical symmetry properties and specular scattering phenomena exhibited by such an array. Our motivation was also prompted by the aforementioned scarcity of relevant data and partly by the encouragement of the late Prof. P. Debye who recognized the significance of such experiments. The data presented in this report were accumulated during the period 1968-1970 in two different buildings at Rensselaer Polytechnic Institute, Troy, New York.

2. ON PERFORMING THE EXPERIMENTS

In former theses, reports, and published works (Lind, et al., 1965; Lind, 1966; Wang, 1968; Wang et al., 1977; Wang and Greenberg, 1978) we have already described the experimental method in great detail. In this report we only supplement these descriptions with topics not previously covered or those important in performing multiple-sphere scattering experiments.

2.1 Target Preparation and Refractive Index Determination

The preparation of scatterers of accurately known size, shape and refractive index is an essential step in performing a microwave scattering experiment. The scattering targets are manufactured by either molding or machining commercially available plastic materials. Since the refractive index of such a material depends only on its density under normal laboratory conditions, the molding technique provides an adequate means of obtaining a scatterer of the desired refractive index. The expandable polystyrene supplied by the Sinclair-Koppers Co. under the trade name Dylite F-40 was found to possess stability, mechanical strength, low humidity-absorption and conductivity. The commercial supply comes in small beads about 0.5 mm in diameter, each with ~7% impregnated volatile material to help expansion when heated. A proper amount of such beads will expand and fuse to each other when heated in an enclosed cavity, transforming them into a strong, smooth-skinned foam filling the mold cavity. Three differently sized spherical cavities (3.2-cm, 3.8-cm, and 4.7-cm diameters) in separate stainless steel blocks were used for molding to facilitate the mold release and to allow heating by steam. A preweighed amount of beads, enough for a near-tight fill was poured into each mold and was steam heated for about 5 hours. Slow expansion in the molding process was preferred to insure the homogeneity of the product target medium. At least nine identical particles for each size were thus fabricated to conduct the multiple-particle experiment.

The refractive index of the target was determined through the dielectric constant measurement of rectangular wave guide samples prepared from the same Dylite F-40 molded in short pieces of the waveguide. The density of such samples spanned that of the target sample so that the refractive index of the latter could be linearly interpolated against the density through the measured values of the former. The measurement technique employs the classical standing-wave method originated by Roberts and von Hippel (1946) and its development in this laboratory (see also Sucher, 1963; Westphal, 1954). The conceptual simplicity, accuracy, and versatility of the method allows the following condensed description.

A standing wave is set up inside a waveguide by an incident wave traveling toward an impedance discontinuity (the shorted waveguide terminal)

and a reflected wave from the same discontinuity. The positions of minima/maxima and the amplitude of the standing wave depend primarily on the geometry of the guide and the dielectric property of the medium containing this wave. Hence, by comparing the standing-wave patterns with and without the dielectric sample in the guide we can deduce the complex dielectric constant $\varepsilon = \varepsilon'-i\varepsilon''$ of the sample. The complex refractive index $m = m'-im''$ then follows Maxwell's relation

$$m^2 = \varepsilon \tag{1}$$

or equivalently

$$\begin{aligned} m'^2-m''^2 &= \varepsilon' \\ 2m'm'' &= \varepsilon'' \end{aligned} \tag{1a}$$

Figure 1 is a schematic of the dielectric measurement. A traveling probe (HP 444A), fitted to a slotted section of a rectangular wave guide (HP X809B), measures the standing-wave profile. The position of the probe along the guide is continuously monitored by a dial gauge (Ames 282M) to an accuracy of ±0.001 cm. One end of the slotted section is short-circuited by a flat brass plate; the other end is connected in series to the klystron oscillator, isolator, frequency meter and a precision attenuator (HP X382A). The oscillator is repeller modulated to produce a 1000-Hz square-wave modulated microwave of carrier frequency f_o = 9.417 GHz, the same frequency used in the scattering set up. The electric field of the standing wave is read by the standing-wave indicator (HP 415B) connected to the probe. Let E_{min} and E_{max} be the minimum and maximum, respectively, of such a field. A rectangular dielectric sample of length l_ε snuggly fits the guide. Let x_o be the distance between the sample surface and the adjacent E_{min} position in the empty portion of the guide. The other sample face touches the short-circuit plate. The propagation constants within the guide are denoted by γ_1 and γ_2 for the empty protion and the sample-filled portion, respectively. Let λ_o be the free-space wavelength, λ_g be that inside the guide of width a and height b, while $\lambda_c = 2a$ is the cut-off wavelength of the same guide. Also let

$$k_o = 2\pi/\lambda_o, \quad k_g = 2\pi/\lambda_g, \quad k_c = 2\pi/\lambda_c \ . \tag{2}$$

If the empty waveguide is sufficiently loss-less and the sample is nonmagnetic, an analysis of the transmission of the TE01 mode microwave shows (Roberts and von Hippel, 1946; Westphal, 1954):

$$\frac{\tan(\gamma_2 l_\varepsilon)}{\gamma_2 l_\varepsilon} = -\frac{i}{k_g l_\varepsilon}\frac{\frac{E_{min}}{E_{max}} - i\tan(k_g x_o)}{1-i\frac{E_{min}}{E_{max}}\tan(k_g x_o)} \ , \tag{3}$$

$$\gamma_1^2 = k_c^2-k_o^2 = -k_g^2 \ , \tag{4}$$

$$\gamma_2^2 = k_c^2-\varepsilon k_o^2 \ , \tag{5}$$

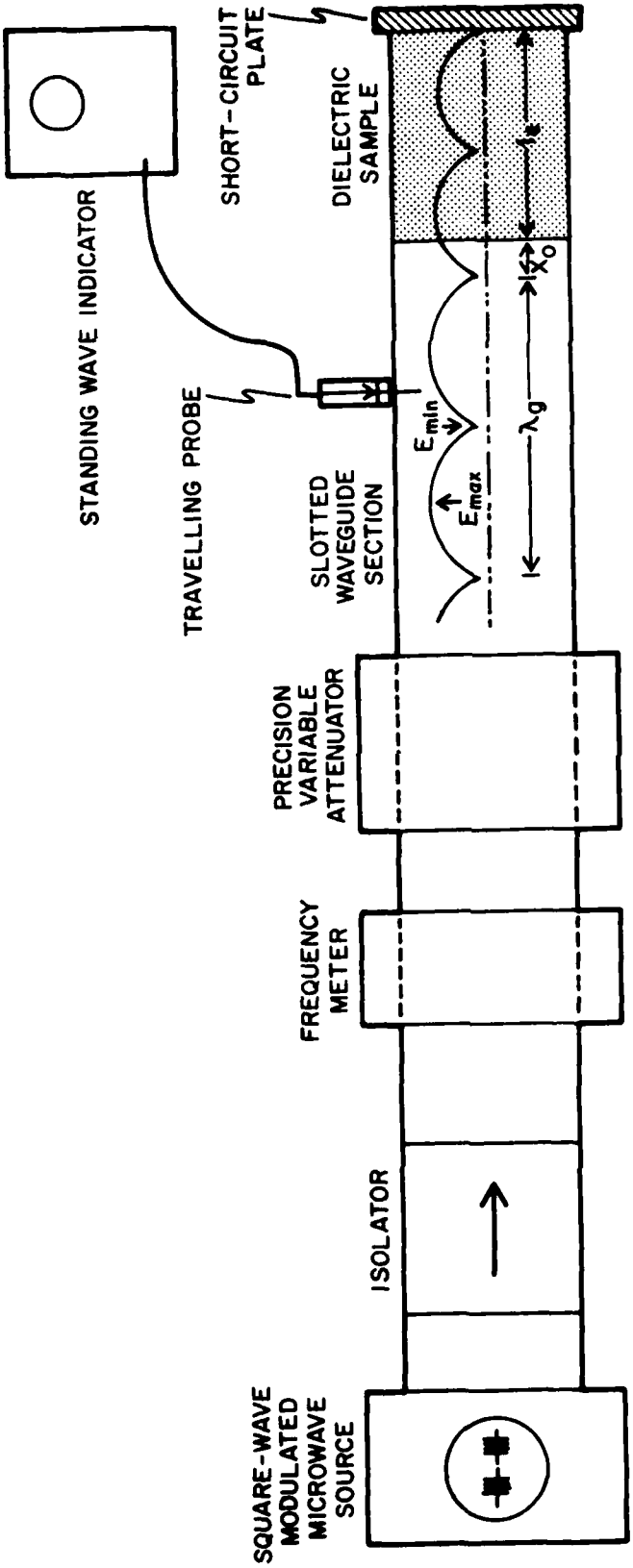

Figure 1. Schematic of the Dielectric Measurement

and therefore

$$\varepsilon = \frac{k_c^2 - \gamma_2^2}{k_c^2 + k_g^2} \quad . \tag{6}$$

Thus, the desired ε is found by (6) in terms of γ_2 which in turn is found by (3) through the measured quantities l_ε, $E_{min}/E_{max} = 1/r$ = inverse standing-wave ratio, x_o, and k_g. In practice, the slotted line is first short-circuited without the dielectric sample, and two successive probe positions, D_R and $D_{R'}$, for E_{min} are recorded. From these, λ_g is found by

$$\frac{1}{2}\lambda_g = D_R - D_{R'} \quad . \tag{7}$$

The sample is then inserted into the guide with one of its end surfaces squarely touching the short-circuit plate. A new E_{min} position, D, is found such that

$$D_R > D > D_{R'} \quad . \tag{8}$$

Since x_o occurs only as $\tan(k_g x_o)$ in (1), a straightforward consideration yields:

$$\tan(k_g x_o) = -\tan\left[k_g(D_R - D + l_\varepsilon)\right] \tag{9}$$

which replaces the measurement of x_o by that of D_R, D and l_ε. The measurement of $r = E_{max}/E_{min}$ is carried out by means of the calibrated variable attenuator (HP X 382A) from which ΔR(in dB), the difference in attenuation to bring E_{min} and E_{max} to the same output level, is obtained. ΔR is directly related to r by

$$r = 10.^{(\Delta R/20.)} \tag{10}$$

This method has the advantage of being independent of the detector characteristics of the probe. With these measured parameters, (3) is solved numerically for $\gamma_2 l_\varepsilon$ by the Newton-Raphson interation method. There are an infinite number of possible roots for $\gamma_2 l_\varepsilon$ arising from the multiple-valued inverse tangent function. The true root is selected from the two sets of roots obtained from two samples of the same material but with different l_ε's. Only the correct root appears in both sets. Better still, if an approximate value of m=m'-im" is known and m" is small, a good starting point (ξ_o, η_o) for the above iteration in the complex plane,

$$\gamma_2 l_\varepsilon = \xi + i\eta \ , \tag{11}$$

is to pick

$$\xi_o = 0 ,$$

$$\eta_o = 2\pi l_\varepsilon \sqrt{\left(\frac{m'}{\lambda_o}\right)^2 - \left(\frac{1}{2a}\right)^2} , \tag{12}$$

a logical choice in view of (5). With the desired $\gamma_2 l_\varepsilon$ and hence γ_2, ε and m follow immediately from (6) and (1). Finally, the measurement error correction on the clearance gap between the waveguide dimension b and the sample thickness d is considered based on the reasoning of the lines-of-force distribution across the dimension b. The corrected value $\varepsilon_c = \varepsilon_c' - i\varepsilon_c''$ is given by

$$\varepsilon_c' = \frac{\varepsilon' d}{b-(b-d)\varepsilon'}$$

$$\varepsilon_c'' = \frac{\varepsilon'' b d}{\left[b-(b-d)\varepsilon'\right]^2} . \tag{13}$$

2.2 Scattering Quantities and Symmetry Relations.

The scattering pattern of a symmetric particle always displays symmetry with respect to its orientation about the incident beam. A careful consideration of this property greatly reduces the number of required measurements. We have already discussed this for the $\theta=0^o$ scattering experiments (Wang, 1968; Wang and Greenberg, 1978) for particles of rotational symmetry, and a short extension to other scattering angles θ will be mentioned for similar particles. A pair of spheres is a symmetric "particle" because the axis of rotation passes through the spheres' centers.

All single-particle-scattering quantities can be defined through the use of the scattering-amplitude matrix $\tilde{S}$, the 4 elements of which are dimensionless complex numbers. This is explained in great detail in van de Hulst's text (1957), and we adhere to his notations throughout this report.

Figure 2 shows the scattering geometry. A linearly polarized incident wave whose electric, magnetic and propagation vectors are $\vec{E}_o$, $\vec{H}_o$ and $\vec{k}_o$, respectively, propagates along the z-axis of a laboratory fixed-coordinate frame (x, y, z) whose y-z plane is chosen horizontal. This plane is called the "scattering plane". The receiver antenna is moved through this plane, at a constant distance from the target site, to observe the scattered wave. The polarizations of the transmitting and receiving antennas were kept vertical (parallel to the x-axis) throughout this report. The pair of spheres, with center-to-center distance s and whose symmetry axis makes an angle χ with $\vec{k}_o$ as shown in figure 2, was always rotated in the y-z plane (the k-H plane) during an experiment. The angle χ is called the "orientation angle." The scattering angle θ is the angular position of the receiving antenna from $\vec{k}_o$ direction, and at which the observation of scattered wave is made. A straight line bisecting the supplement of θ in the y-z plane is called "bisectrix", and a plane containing this bisectrix and orthogonal to the y-z plane is called the "bisectric plane".

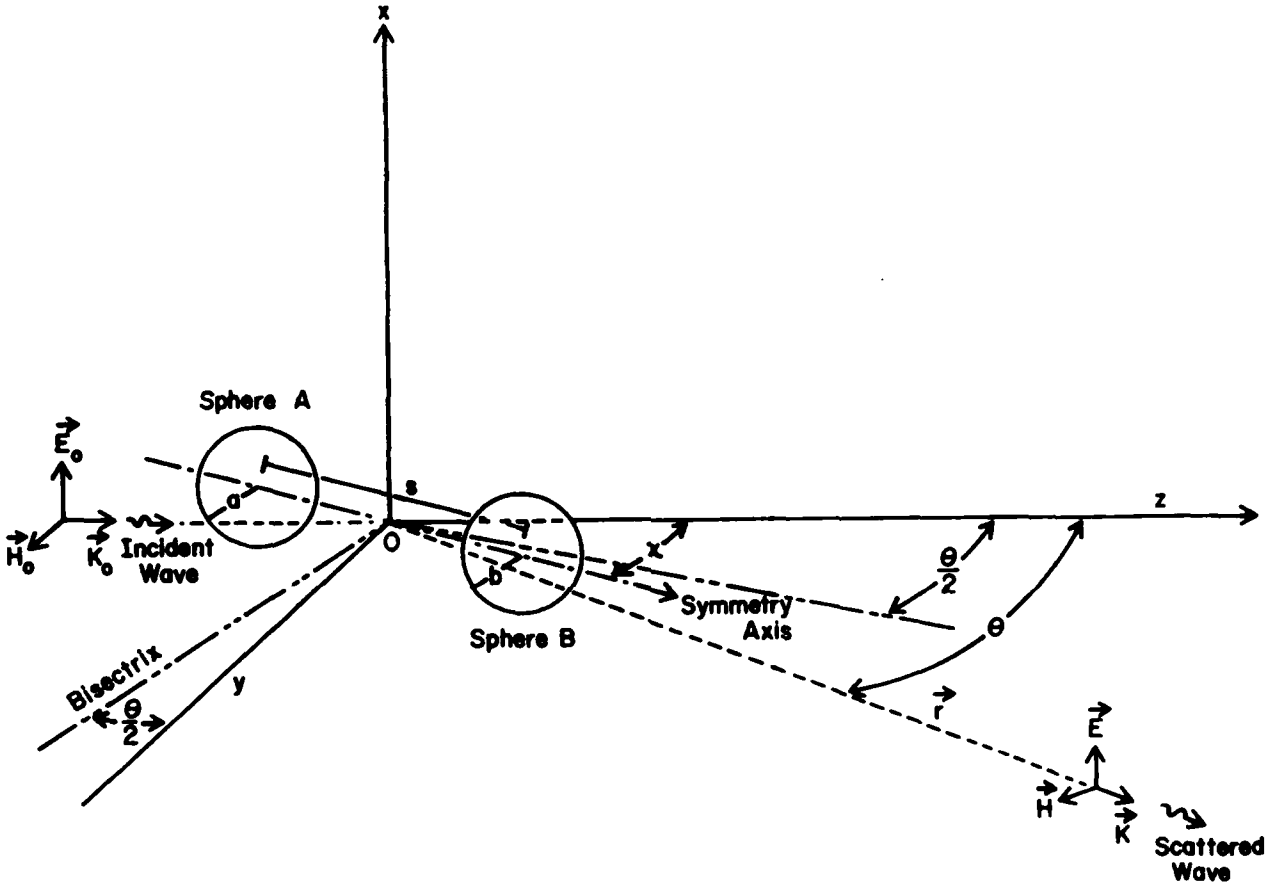

Figure 2. Cartesian Coordinates (x,y,z), Scattering Angle θ, Target-Orientation Angle χ and the Mutual Separation s Which Specify the Geometry of Scattering for a Two-Sphere Ensemble

Given an arbitrary scatterer, van de Hulst (1957) explained that there existed four related particle orientations with respect to the incident polarization in which $\tilde{S}$ at each orientation could be represented by the same set of matrix elements, S_1, S_2, S_3, and S_4:

Orientation a Orientation b Orientation c Orientation d

$$\tilde{S}_a = \begin{pmatrix} S_2 & S_3 \\ S_4 & S_1 \end{pmatrix} \quad \tilde{S}_b = \begin{pmatrix} S_2 & -S_4 \\ -S_3 & S_1 \end{pmatrix} \quad \tilde{S}_c = \begin{pmatrix} S_2 & -S_3 \\ -S_4 & S_1 \end{pmatrix} \quad \tilde{S}_d = \begin{pmatrix} S_2 & S_4 \\ S_3 & S_1 \end{pmatrix}$$

Orientations b, c and d are achieved from the orientation a through: 180° particle rotation about the bisectrix, mirroring the particle with respect to the scattering plane and mirroring the particle with respect to the bisectric plane, respectively. For a rotationally symmetric particle the immediate consequences of these relations are the following:

(1) If the rotation axis lies in the scattering plane, the orientations (a) and (c) are identical. Equating the $\tilde{S}$ matrix elements for both positions we have $S_3=-S_3$ and $S_4=-S_4$, which is true if and only if $S_3=S_4=0$. With zero off-diagonal elements in the $\tilde{S}$ matrix, there is no cross-polarized component in the scattered wave.

(2) As the symmetry axis is rotated in the scattering plane, the scattered signal varies periodically with respect to the χ variation. The pattern is symmetric about the bisectrix with period $\pi/2$. That is, the symmetry axis needs only be swept in the χ interval:

$$\frac{\theta}{2} \leq \chi \leq \frac{\theta}{2} + \frac{\pi}{2} . \tag{14}$$

This follows from the property $S_3=S_4=0$ under this rotation. Outside the range of χ, one can always find a reciprocal orientation position inside the χ range (equally spaced from the bisectrix) whose corresponding orientation has the same S_2 and S_1.

2.3 On Suspending, Orienting and Separating Multiple Spheres.

Since the objective is to find the precise scattering signature of an ensemble of spheres as a function of its geometrical configuration, an ideal suspension and orientation mechanism should add little to the true scattering from the ensemble and should allow the quick, accurate and reproducible positioning of the ensemble to the desired orientation. It was found that a skillful employment of the orientation device described in Lind's thesis (1966) with only a few modifications would meet most of the requirements.

Two small nylon eyelets were anchored onto a pair of diametrical poles of each sphere, and thin nylon strings passing through each eyelet allowed the assembling of multiple spheres. Appropriate selection of the lengths and path sequence of these strings enabled one to achieve the desired geometrical shape of the ensemble when it was hoisted into the incident beam; both the upward and downward pull of the nylon threads in the orientation mechanism itself tightened these strings to hold the individual spheres in place. Since each sphere could be slid a little along the strings passing through its own eyelets, the precise relative positions of spheres were adjusted manually. This practice worked particularly well for 2 spheres in a discrete set of mutual separations and for 4 to 8 spheres forming a contacting square or cubic array, and such arrays could be rotated azimuthally without deformation.

Continuous separation of 2 spheres for the $\theta=0^{\circ}$ measurements were performed only for the orientation where 2 spheres were aligned along the incident direction. In this case the first sphere was positioned in the normal target site of the orientation mechanism. The second sphere was suspended, like a pendulum bob, from the pivoting point of the orientation mechanism near the ceiling by means of a separate nylon string. Another thin, long, nylon string was passed through 2 eyelets of this second sphere, the string ends separately going through two-floor-level eyelets straddling (but "downstream" from) the incident beam. This string also served as a stabilizing agent of the movable sphere, and the continuous separation of 2 spheres was accomplished by simultaneously pulling both string ends.

These target separation/orientation techniques have remarkable simplicity, speed, and reliability if the following precautions are taken: (1) The ensemble should stay within the acceptable region of the incident beam. Thus, the separation distance between 2 spheres can not be indefinitely large. (2) For the discrete 2-sphere separation case, the target height is dependent on the separation distance. (3) For the continuous separation case, it is somewhat difficult to hold both spheres at the same height. The sphere being pulled was observed to go higher than the other by as much as its own radius at a separation distance of five sphere diameters if care was not exercised during the pull. (A servo controlled motor-gear mechanism was later built which seemed to remedy this difficulty.)

We have to remark that such an ensemble of string-assembled multiple spheres can only be rotated azimuthally without geometrical deformation using the present orientation mechanism.

2.4 More Remarks on Antennas and Sources of Experimental Errors.

We have already reported the important role of antennas in indoor precision measurements (Wang et al., 1977; Wang and Greenberg, 1978). In combination with a good anechoic chamber, the antenna's design not only determines the size range of scatterers that can be investigated, but can also be used to reduce the unwanted background radiation. Careful alignment of the transmitting and receiving antennas insures the symmetricalness of the radiation and reception patterns about the beam axes. During the period when the data in this report was taken, the antenna alignment could only be carried out by adjusting the orientations of both transmitting and

receiving apertures to yield the maximum received signal. Subsequent fine adjustments were made to see if at $\theta=0^o$ the amplitude-phase plot of a small sphere would retrace as the sphere was moved across the beam. If we changed both the incident and receiving polarizations through 90^o after this adjustment was made, however, an unacceptable retrace was observed. The mechanical difficulty of precisely keeping the dipole-disk assemblies in the geometrical centers of each antenna as they were rotated explains why both polarizations were kept fixed (vertical) throughout this experiment.

Antenna-target multiple scattering is another source of experimental error for $\theta=0^o$ measurement and causes systematic errors even in single-sphere runs. In addition to the incident plus singly scattered waves arriving at the receiver antenna, we have 2 first-order multiple scattered signals, neglecting the smaller higher order multiple reflections. These 2 signals go through the path sequences transmitter-scatterer-transmitter-receiver and transmitter-receiver-scatterer-receiver, respectively. Analyses (Lind, 1966; Wang, 1968) showed that the percentage error of the amplitude and phase measurements at $\theta=0^o$ increased linearly with the ratio $|S(\pi)|/|S(0)|$ of the target, decreased linearly with the antenna-target separation, and was proportional to the backscatter cross sections of antennas. With the latter two parameters fixed, the error is seen to be less for targets with smaller $|S(\pi)|/|S(0)|$ ratio like the softer particles made from expanded polystyrene and larger for harder particles prepared from acrylic material. Errors in the latter case may be as large as $\sim$10% in amplitude and $\sim 12^o$ in phase). A general remedy for this source of error is not yet well established.

A controversial requirement on the minimum antenna-target separation distance (Silver, 1949, 1962; Beard et al., 1962; Hansen and Bailin, 1959; Rhodes, 1954) did not seem to have a critical effect on the measurements. We employed only about half of the far-zone distance in this investigation.

3. EXPERIMENTAL RESULTS

3.1 Forward Scattering ($\theta=0^o$).

Each P, Q plot in this section is a cartesian representation of the complex forward scattering amplitude S(0) as a function of orientation angle χ or the mutual separation $ks=2\pi s/\lambda$ of the particle ensemble (see fig. 2). In the complex plane the dimensionless P and Q components are:

$$P = \frac{4\pi}{k^2 G} \text{Im}\{S(0)\} \quad , \quad Q = \frac{4\pi}{k^2 G} \text{Re}\{S(0)\} \quad , \tag{1}$$

where G is the appropriate geometrical cross section of the ensemble, *the sum of geometrical cross sections of the component spheres*, and Q is the so called "extinction efficiency". A vector drawn from the coordinate origin to each χ (or ks) position along the curve yields the complex value of S(0) at χ (or ks). The phase shift $\phi(0)$ of the $\theta=0^o$ scattered wave is given by the angle between this vector and the P axis, while the projection of this vector into the calibrated Q axis gives the extinction efficiency (C_{EXT}/G). The length of this S(0) vector represents the absolute value $|S(0)|$, and its numerical value is obtained by comparing this length with that of the "standard" or calibration

vector (obtained from a sphere) provided in each plot. The numerical value of $|S(0)|$ for the calibration sphere is given in table 1.

The P, Q plots in this subsection are subdivided according to number, size, refractive index and method of separation of the component spheres, the parameters of which are listed in each P, Q plot and also tabulated in Table 1 along with relevant Mie scattering quantities.

3.1.1 Arrays of 2 Identical Spheres in Discrete Steps of Mutual Separation and of Rotation in the Incident k-H Plane.

Figures 3A-3I, 4A-4H, and 5A-5F are the experimental P, Q plots for 3 pairs of 2-sphere ensembles. The pairs differ from one another only in the size of the component spheres. Target parameters and the mutual separation ks is shown in each plot. At the orientation k, the array is aligned on the incident direction. It is then continuously rotated through 90° in the k-H plane of the incident wave to display the continuous curve, finally arriving at the orientation H where the array is perpendicular to the incident k vector. Fiducial marks along the curve denote the orientation angle χ.

All component spheres have refractive indexes near m=1.365 and resemble those of water or ice in the optical spectrum. Such a 2-sphere ensemble displays the simplest-looking P, Q plot among those made by other multiple spheres, but a detailed explanation is not yet available. However, some striking phenomenological features are evident: (a) The phase shift $\phi(0)$ of the $\theta=0^\circ$ scattered wave is invariably larger at the k-orientation than at the H orientation for these particle sizes. (b) At the H orientation, $\phi(0)$ is about the same as that of a component sphere, but the magnitude $|S(0)|$ is about twice as large; i.e., the two spheres scatter the incident wave more or less independently. (c) As the array is rotated from k to H orientation, the tip of S(0) vector generates a clockwise arc or spiral, converging toward the H orientation faster as χ increases. At $\chi=60^\circ$, the S(0) vector is already near that at $\chi=90^\circ$, the H orientation. Crudely speaking, one sphere emerges out of the other's shadow. (d) As the mutual separation ks increases, the above feature (c) is more pronounced, resulting in the shrinking of the overall size of the P, Q plot. This effect is a vivid representation of the decrease in dependent scattering.

3.1.2 Arrays of 2 Dissimilar Spheres in Discrete Steps of Mutual Separation and of Rotation in the Incident k-H Plane.

P, Q plots of an array of 2 different sized spheres being rotated in the k-H plane are shown in figures 6A-6F for six steps of separation ks. In addition to a standard calibration sphere, the vector S(0) of each component sphere was measured independently. The results are shown in the same P, Q plot as 2 dotted lines marked SPHERE 1 and SPHERE 2, respectively. All characteristic features in the previous section 3.1.1 apply here also. Notice, in particular, that at H orientation the S(0), vector of the array is nearly equal to the vector sum of the individual spheres.

P, Q plots for another 2-sphere array whose component spheres are nearly the same in size but different in refractive index are shown in figures 7A-7H

Table 1. Characteristics of Spherical Targets

Target parameters and several scattering quantities by Mie theory for each spherical particle are shown: $x=2\pi a/\lambda$; a=radius; m=complex refractive index; $|S(0)|$=amplitude of the $\theta=0^{\circ}$ scattered wave; $\phi(0)$=phase shift in degrees of the $\theta=0^{\circ}$ scattered wave; $i(0)=|S(0)|^2$; $i_1(90)$=perpendicular scattering intensity component at $\theta=90^{\circ}$; i(180)= backscatter intensity.

Sphere ID No.	x	Material	m	$\|S(0)\|$	$\phi(0)$	i(0)	$i_1(90)$	i(180)
Std #1	4.993	Expanded Polystyrene	1.267	21.38	54.6	457.2	1.012	1.759
Std #4	6.241	"	1.258	36.06	66.7	1301.0	1.835	1.691
Std#13	4.276	"	1.254	13.57	43.8	184.1	0.7688	0.3535
	3.120	"	1.365	7.87	44.8	61.94	0.9834	0.4629
	3.752	"	1.366	12.88	54.6	165.9	1.727	1.569
	4.678	"	1.363	21.97	69.2	482.6	1.324	3.835
	1.237	Acrylic	1.610-i0.004	0.8447	17.3	0.714	0.318	0.1195
	1.368	"	"	1.169	20.7	1.367	0.468	0.1119
	1.856	"	"	3.015	41.5	9.090	0.809	0.2578
	2.166	"	"	4.252	48.2	18.08	0.594	0.7096
	3.085	"	"	10.08	71.7	101.7	1.739	3.210
	3.733	"	"	13.87	91.2	192.4	3.773	4.651
	4.341	"	"	17.63	106.4	310.7	1.051	7.891
	4.980	"	"	19.53	113.9	381.6	6.674	30.29

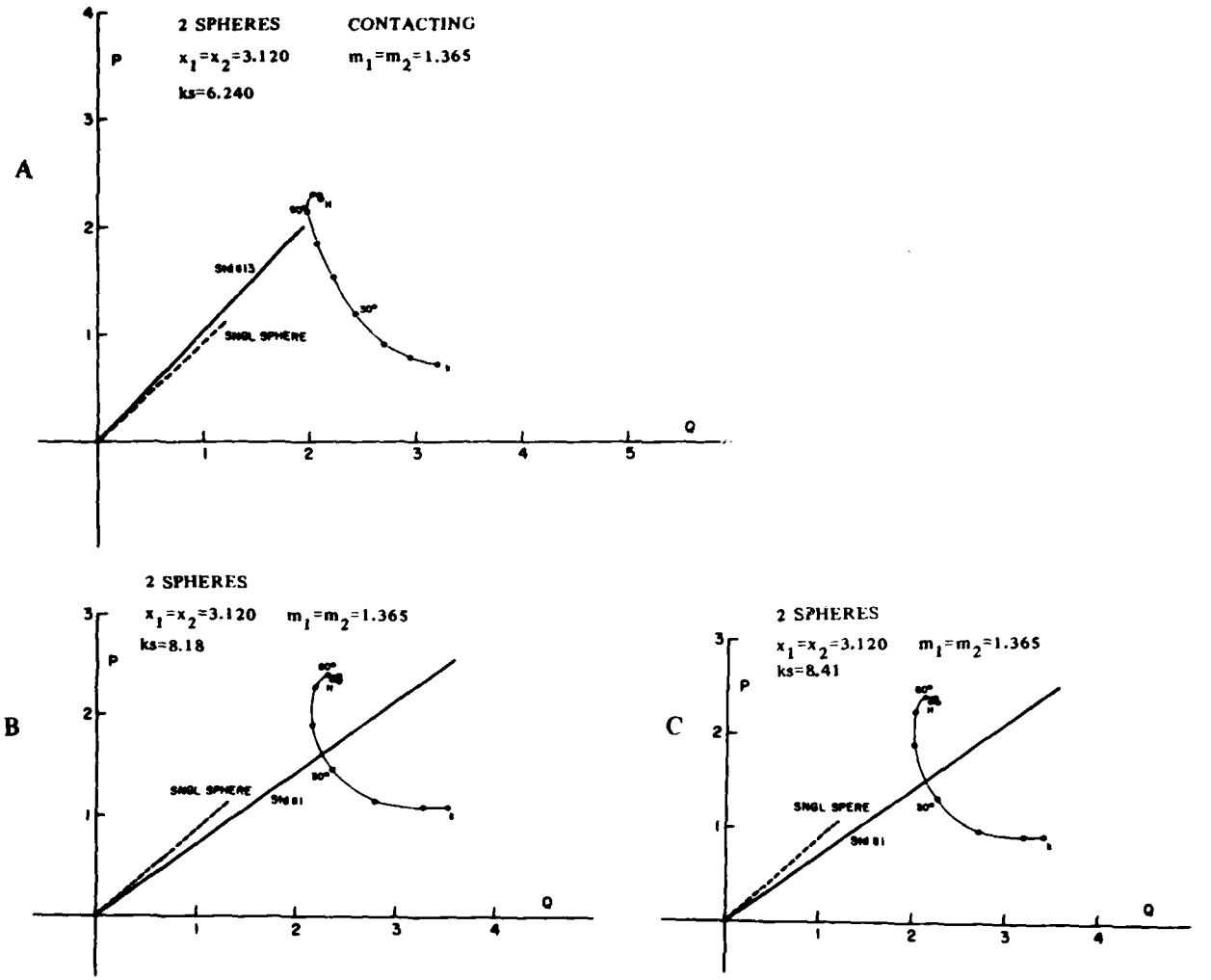

Figure 3, A to C. Plots of θ=0° Scattering by an Array of Two Identical Spheres as the Array Orientation (χ) Is Continuously Varied. The separate graphs refer to discrete sphere-separations (ks). See sections 3.1 and 3.1.1.

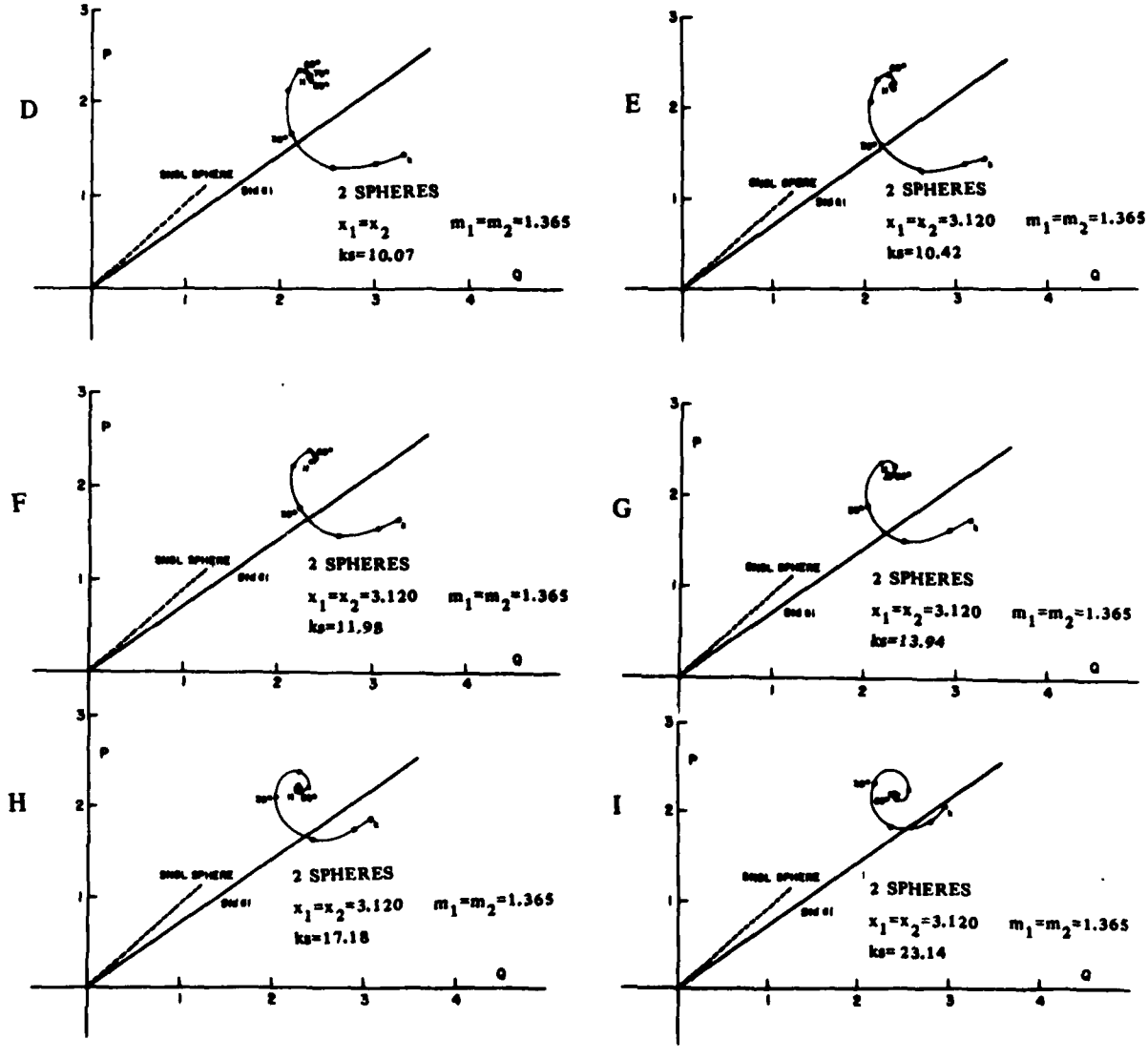

Figure 3, Contd, D to I

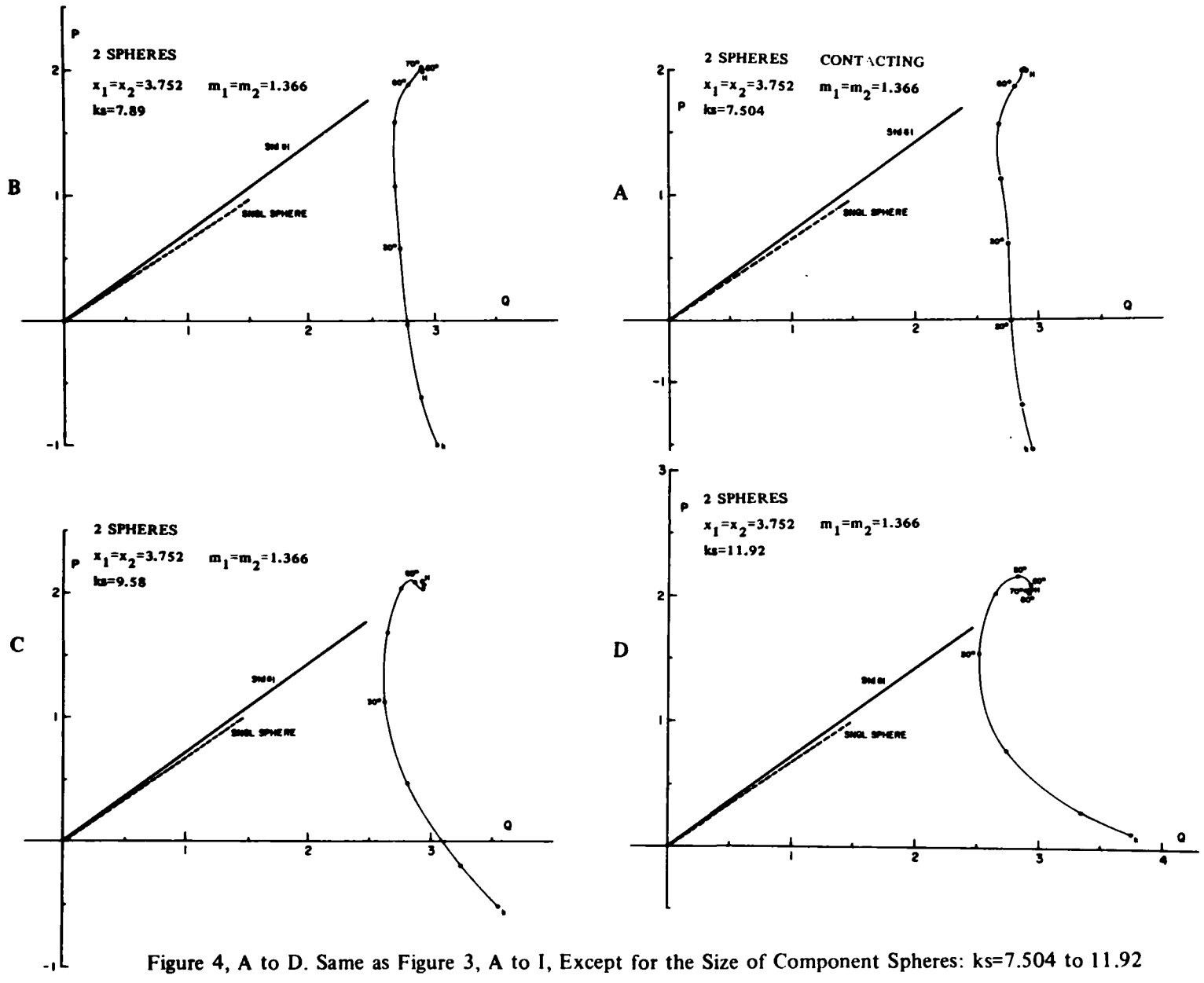

Figure 4, A to D. Same as Figure 3, A to I, Except for the Size of Component Spheres: ks=7.504 to 11.92

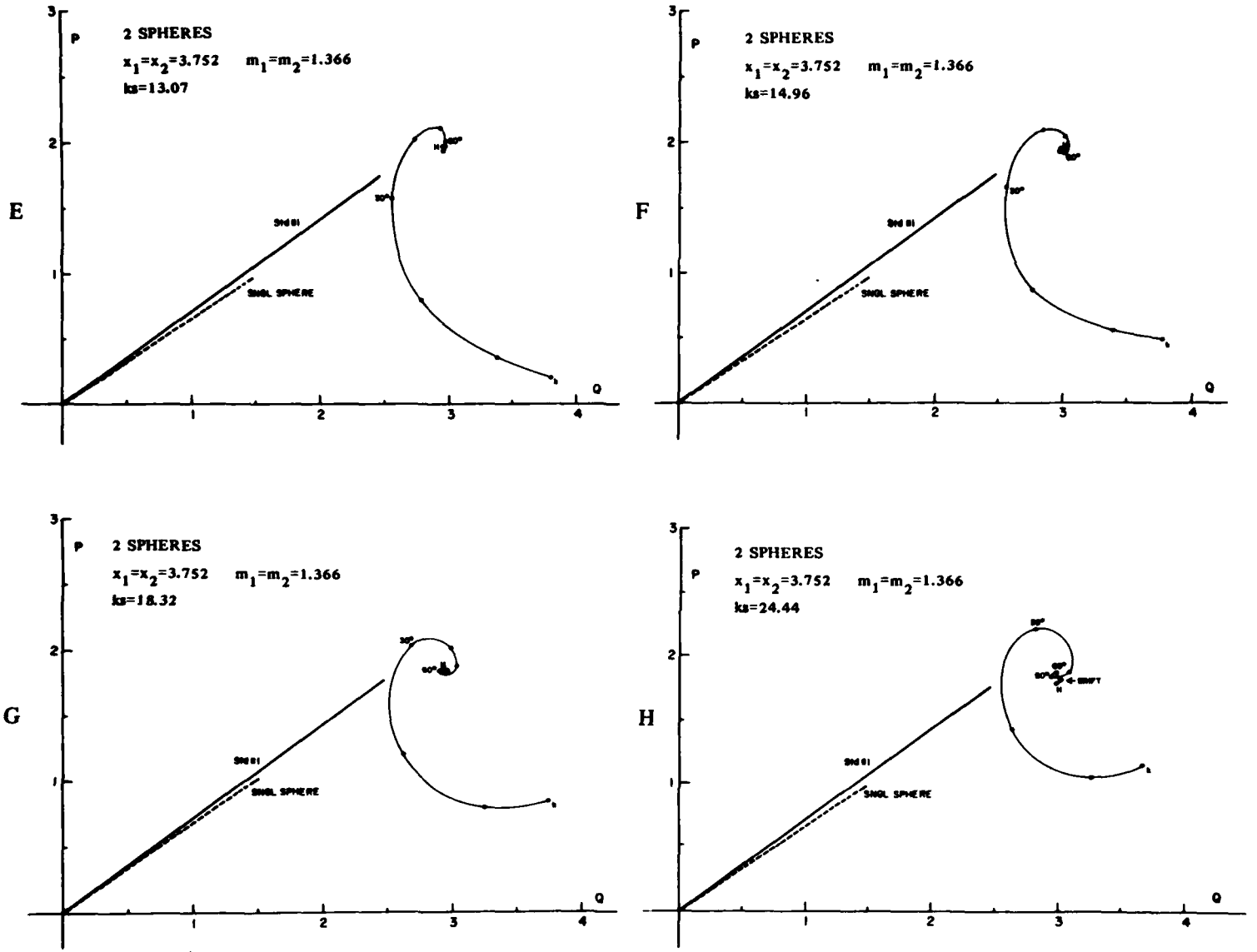

Figure 4, E to H. Same as Figure 3, A to I, Except for the Size of the Component Spheres: ks=13.07 to 24.44

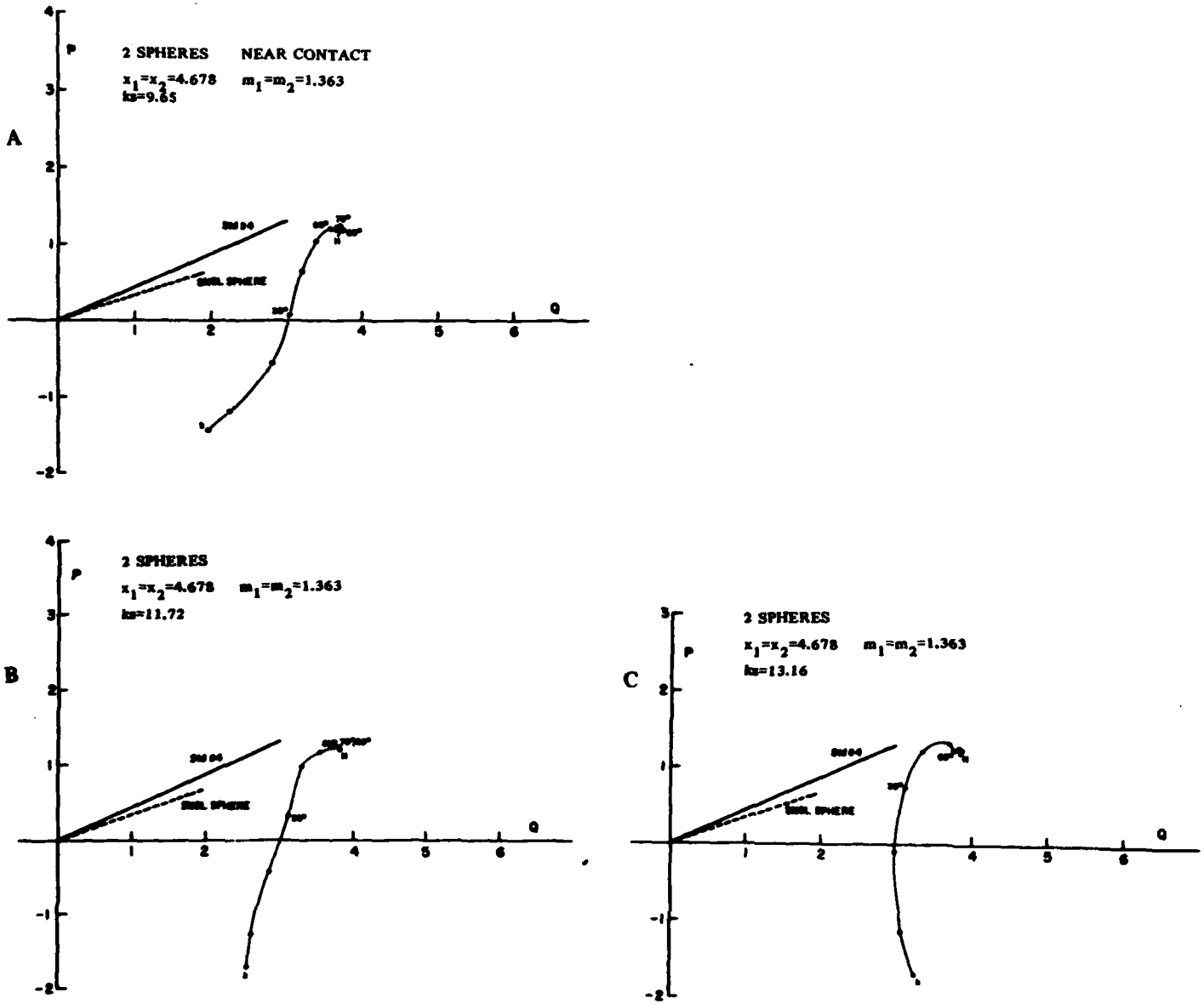

Figure 5, A to C Same as Figure 3, A to I, Except for the Size of the Component Spheres: ks=9.65 to 13.16

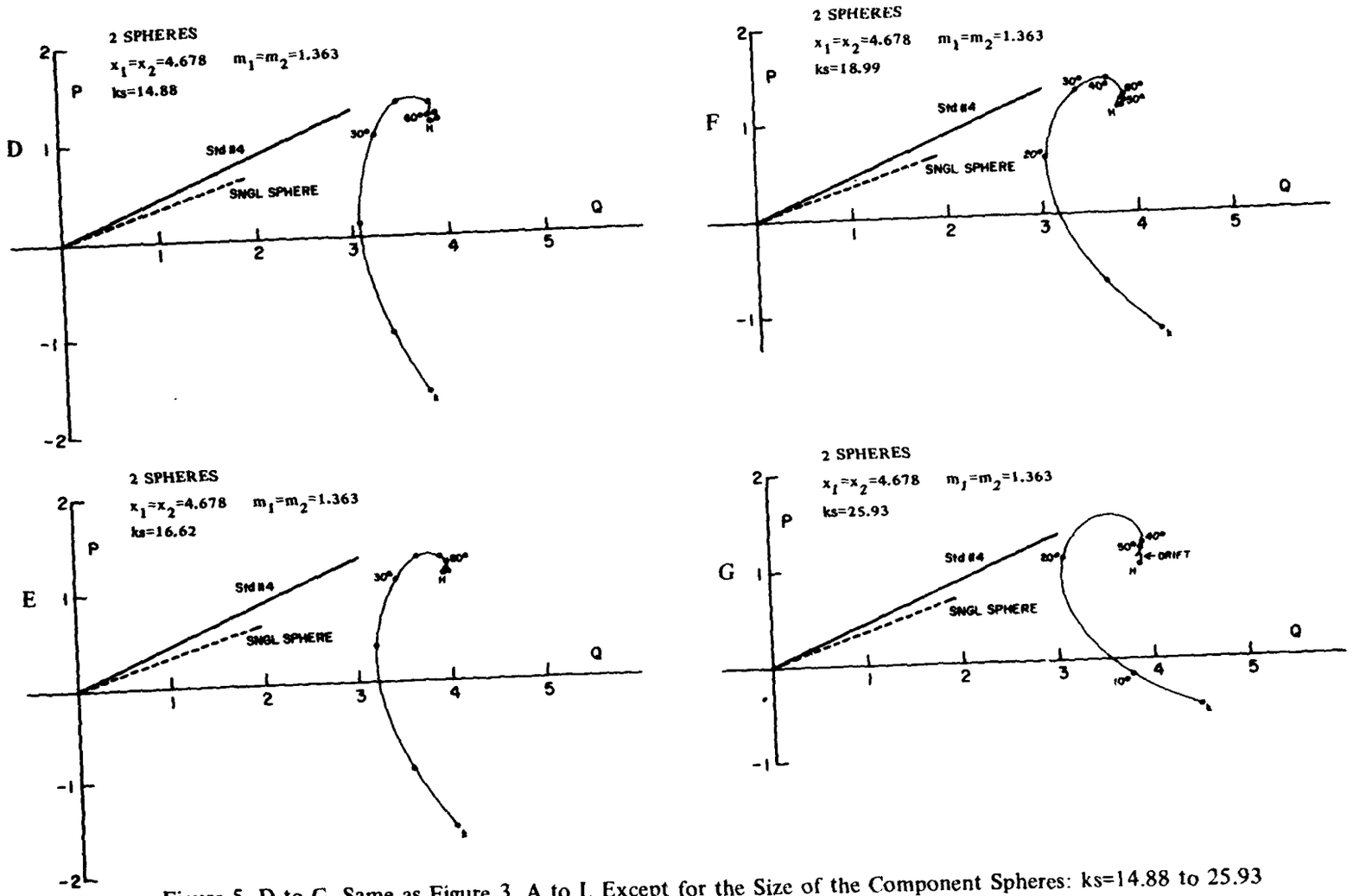

Figure 5, D to G. Same as Figure 3, A to I, Except for the Size of the Component Spheres: ks=14.88 to 25.93

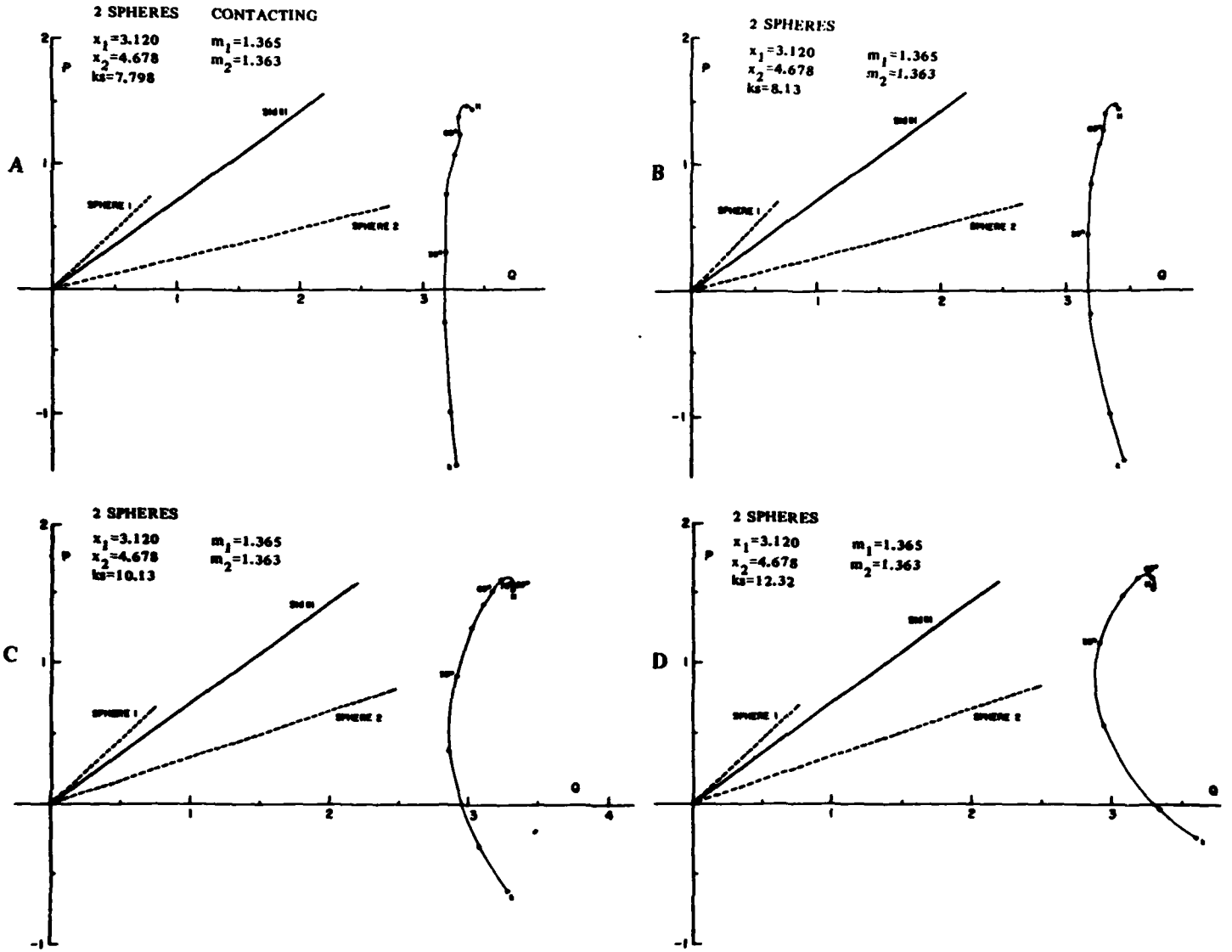

Figure 6, A to D. P, Q Plots of θ=0° Scattering by an Array of Two Unequally Sized Spheres as the Array Orientation (χ) Is Varied. The separate graphs refer to discrete steps of sphere-separation (ks). See sections 3.1, 3.1.1 and 3.1.2

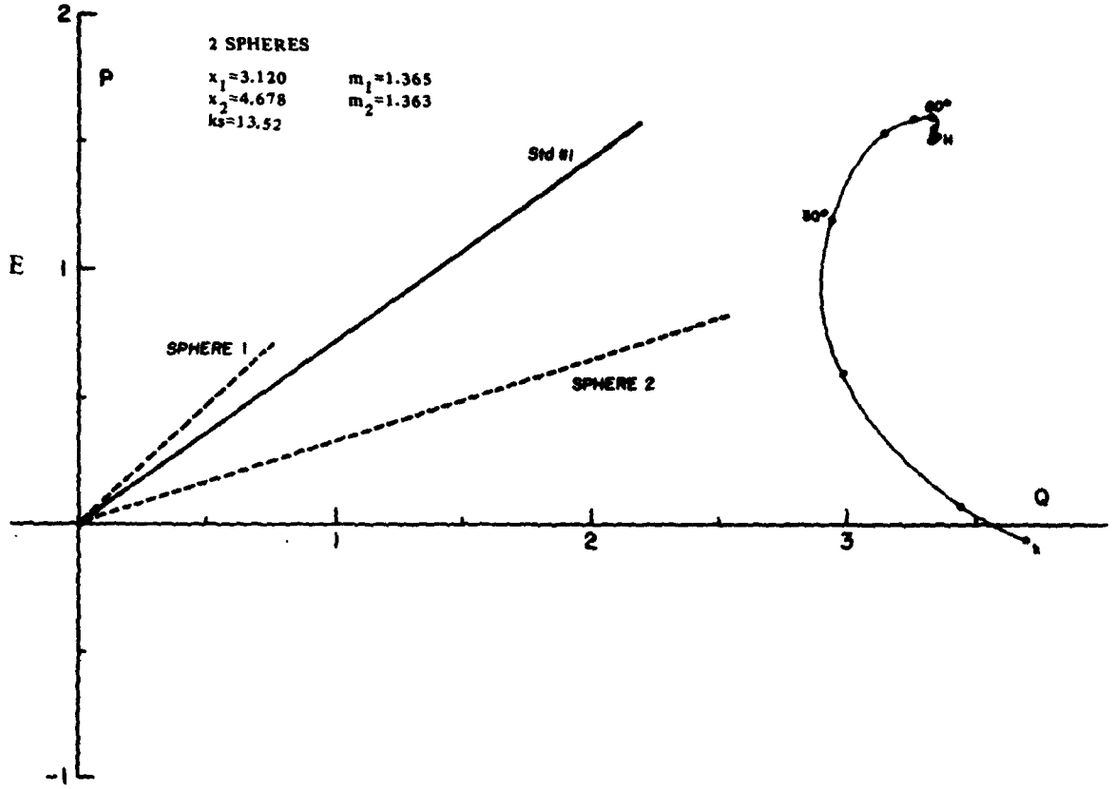

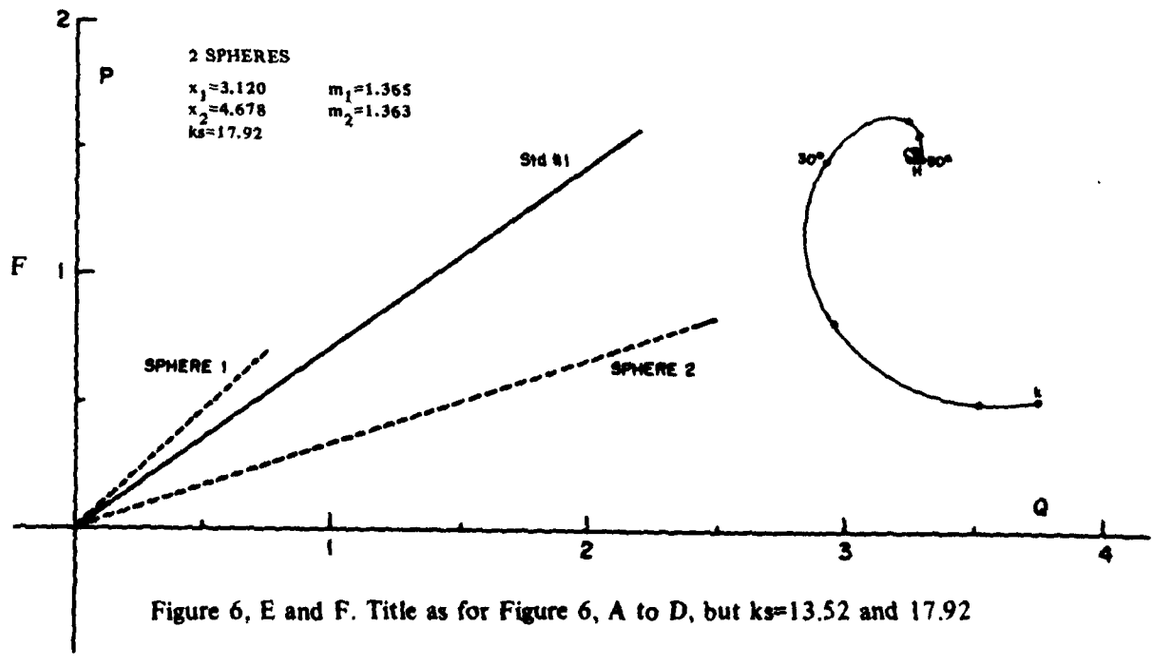

Figure 6, E and F. Title as for Figure 6, A to D, but ks=13.52 and 17.92

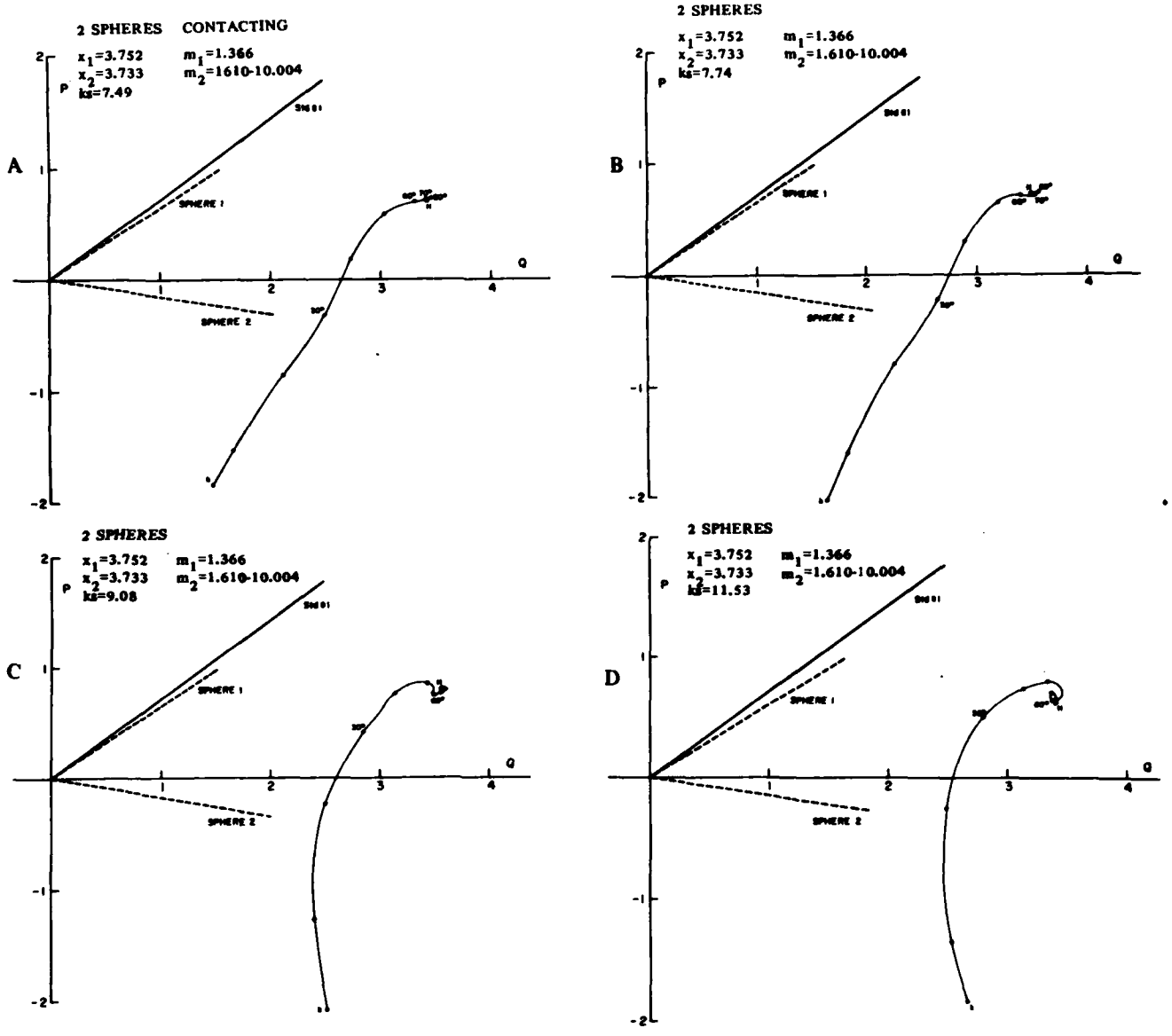

Figure 7, A to D. Same as Figure 6, A to D, Except the Two Spheres Here are Dissimilar in Their Refractive Indexes: ks Varies from 7.49 to 11.53

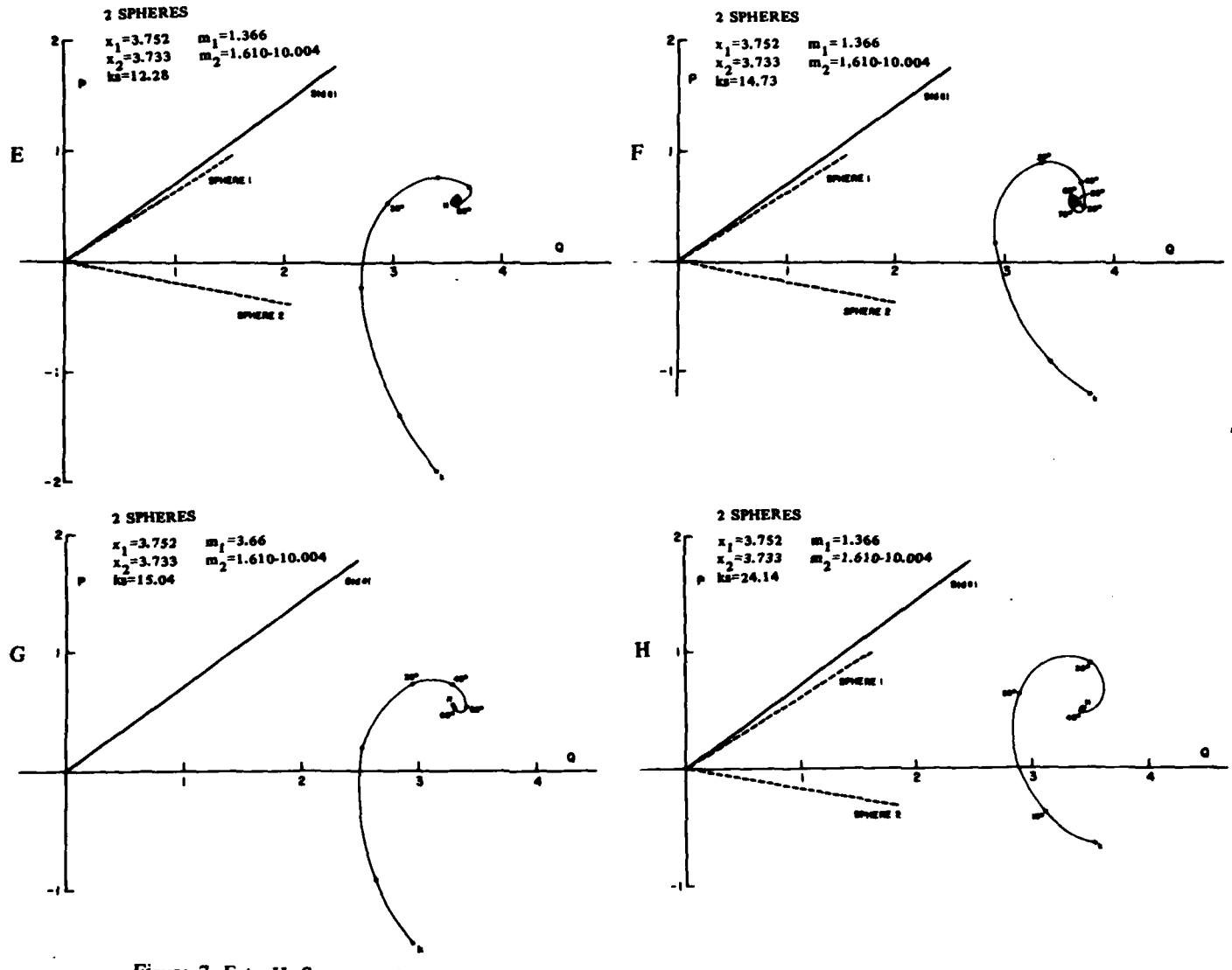

Figure 7, E to H. Same as Figure 6, A to D, Except the Two Spheres Here are Dissimilar in Their Refractive Indexes: ks Varies from 12.28 to 24.14

Table 2. Comparison of Experimental and Theoretical $|S(0)|$'s AND $\phi(0)$'s

The experimental $\theta=0^\circ$ scattering amplitude $|S(0)|$ and phase shift $\phi(0)$ for each contacting 2-sphere array at the broadside incidence (H) orientation is compared with the corresponding theoretical predictions resulting from the summation of independent scattering by these 2 Mie spheres. All spheres are of acrylic material, with refractive index m=1.610-i0.004.

Array No.	x Size of Component Sphere	Experimental		Theoretical	
		$\|S(0)\|$	$\phi(0)$	$\|S(0)\|$	$\phi(0)$
1	1.237	1.78	21.2°	1.689	17.3°
2	1.368	1.93	22.5°	2.338	20.7°
3	1.856	5.40	33.5°	6.030	41.5°
4	2.166	8.49	46.2°	8.504	48.2°
5	3.085	36.25	53.0°	20.16	71.7°
6	3.733	28.15	93.8°	27.74	91.2°
7	4.341	38.68	106.6°	35.26	106.4°
8	4.980	41.75	115.0°	39.06	113.9°

for 8 steps of center-to-center separation ks. In the optical spectrum, the refractive index of one component sphere resembles that of ice or water, while the other that of silicates. Identical P, Q plots were observed in both k-H plane rotations whether the silicate particle was initially (at k orientation) placed in the shadow of the ice particle or vice versa. Here again the conspicuous feature of the minimum dependent scattering effect is obvious at the H orientation; the resultant vector S(0) falls in the vicinity of the vector sum of the S(0) vectors of the (independent) component spheres at this orientation. Characteristics (a), (c) and (d) described in Section 3.1.1 are also observed here.

3.1.3 Contacting 2 Identical Spheres of Eight Array Sizes.

The scattering by 8 pairs of 2 contacting identical spheres of acrylic material, each pair differing from the others only in size, were measured separately to give the signatures shown in figures 8A-8H. Notice that each pair has the same volume as that of a prolate spheroid of elongation 2:1 whose semi-minor axis is equal to the sphere radius. Due to the high refractive index of these particles, corresponding to that of silicate particulates in the optical spectrum, we also notice marked differences from the P, Q plots of dylite (expanded polystyrene) particles in preceding sections. It was rather difficult to prepare more than two identical spheres from the commercially machined sphere stock, and it was therefore impractical to do the (independent) component sphere runs quickly enough before the microwave compensation drift became perceptible. In addition, these silicate-type spheres have a high back to forward scattering ratio ($i(\pi)/i(0)$) as indicated by table 1, and hence the measurements may contain pronounced errors due to the antenna-target multiple scatter effect (Lind, 1966; Wang, 1968). We could not correct this effect by performing the then purported array-pulling technique without seriously deforming the array geometry. Hence, we reproduce here the direct observations without such technical modifications.

A closer analysis of these P, Q plots and a comparison with those by ice-like particles in the preceding sections reveal, however, the following similarities and contrasts: (a) At the H orientation, where an array presents its broadest face with respect to the incident direction, S(0) of the array is close to that of the vector addition of S(0) vectors of component spheres, with the exception of two particular arrays shown in figures 8C and 8E. This vector addition of independent scattering as obtained by Mie theory is compared with the observations as shown in table 2. (b) For smaller array sizes, figures 8A-8E, the tip of the S(0) vector generates a clockwise arc/spiral as the array is rotated from k to H orientation. As the size increases further, this trend disappears, resulting in a complex variation with respect to the changing orientation. Such a P, Q plot bears little resemblance to that obtained from a similarly sized array of ice-like particles with lower index of refraction. (c) For all sizes, both the magnitude $|S(0)|$ and phase $\phi(0)$ change most rapidly during the orientation change $10^{\circ} \leq \chi \leq 60^{\circ}$, and at $\chi=60^{\circ}$ S(0) already converges to that near $\chi=90^{\circ}$, the H orientation. (d) If an array is properly sized as in figure 8F, the total cross section of the array may vary by a factor ~ 7 during such a k-H plane rotation.

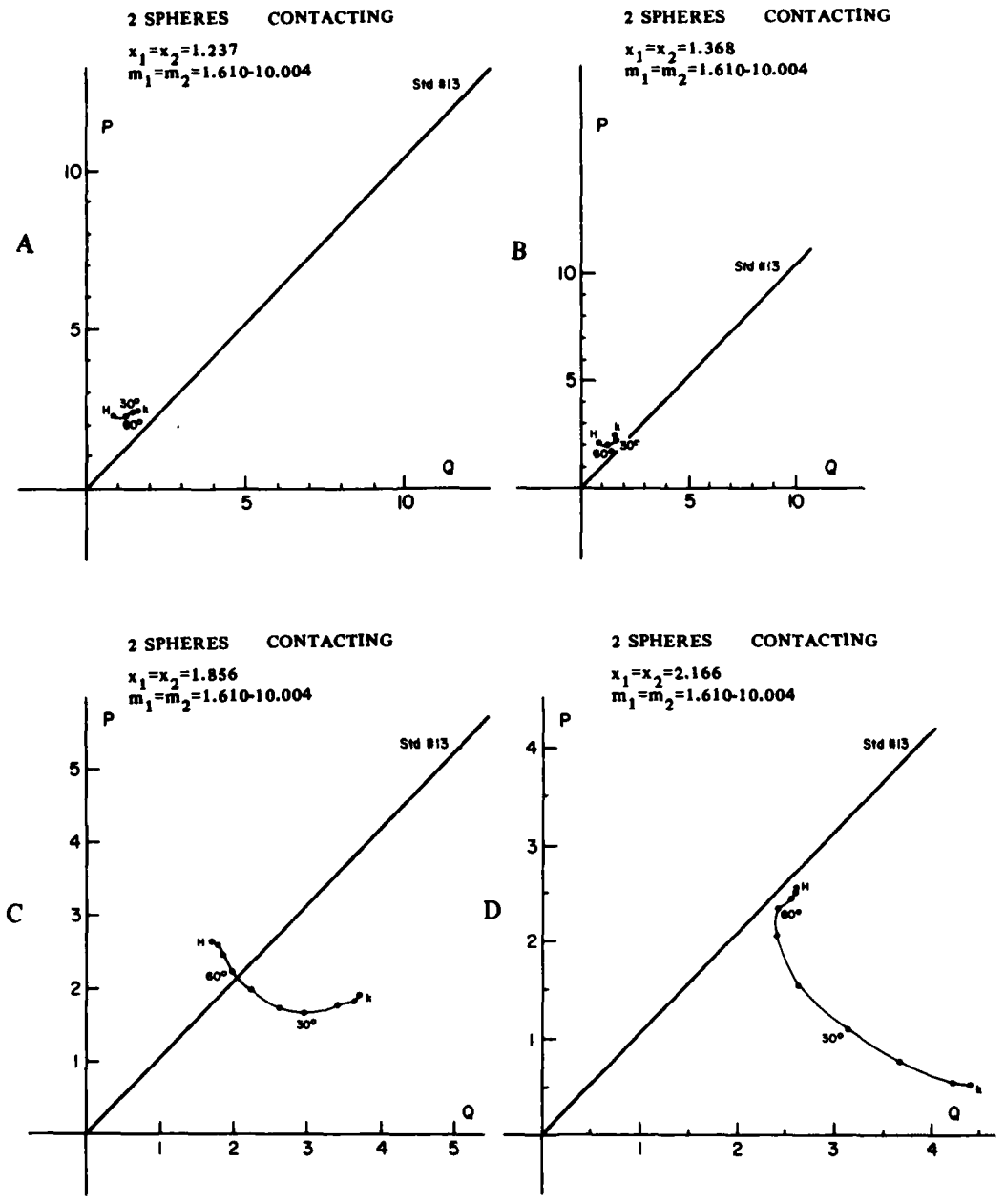

Figure 8, A to D. P, Q Plots of $\theta=0°$ Scattering by Arrays of Contacting Two Identical Spheres as the Array Orientation (χ) Is Varied. The separate graphs refer to arrays of different size. See sections 3.1 and 3.1.3

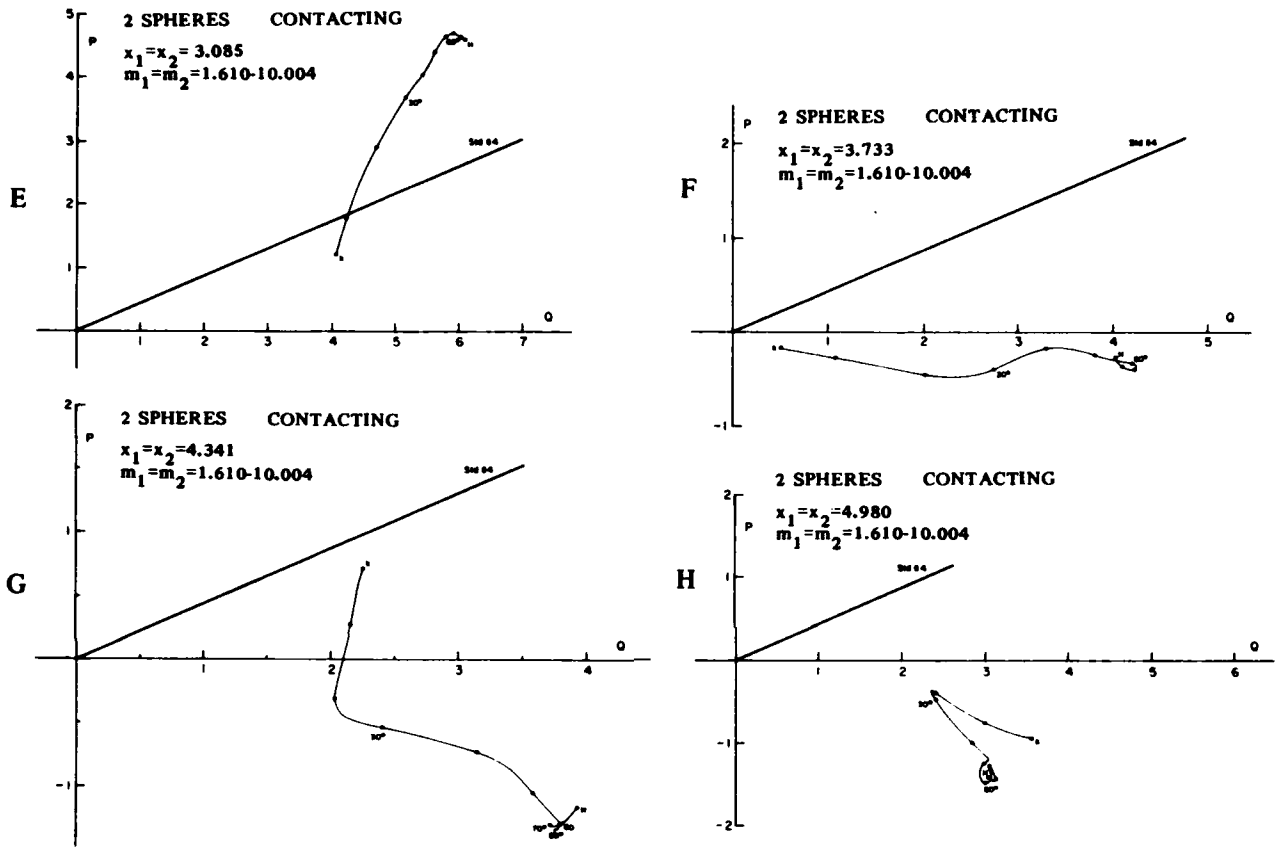

Figure 8, E to H. Same as Figure 8, A to D but x_1,x_2 Varies from 3.085 to 4.980

3.1.4 Continuous Separation of 2 Identical Spheres Along Incident Direction.

In this section, we present a detailed investigation of the dependent scattering process when 2 spheres are continuously pulled apart along the direction of the incident radiation, thereby recording a P, Q plot as a function of separation. In this special orientation, one sphere is always in the geometrical shadow of the other, and a more coherent understanding of their mutual dependence may be possible. This was done for 4 pairs of spheres, one of which has ice-like particles (fig. 9A), while others resemble silicates (figs. 9B-9C). Target parameters can be found in each figure as well as in table 1. The running numbers in each P, Q plot denote the mutual separation $ks=2\pi s/\lambda$, where s is the center-to-center distance between two spheres.

Some striking phenomena observed in these P, Q plots are: (a) In general, the tip of the S(0) vector travels in a counterclockwise curve in each P, Q plot as ks increases, converging toward a limit corresponding to $ks=\infty$ with ever decreasing speed. This limit represents the summation of independent scattering by two spheres, as shown in each plot by an extended straight section, half of which (the solid section) being the S(0) vector of an isolated single sphere as measured during the same experimental run. (b) If the center-to-center distance between two spheres (s) is less than about 1.5 diameters of a sphere, the P, Q vs s plot is a featureless curve. Beyond this, however, the plot exhibits wavy structures superimposed on a main locus, indicating the S(0) vector of the array oscillates about a median function of s. (c) The extinction cross section of the array is not always a monotonous function of s. Depending on the size and refractive index of component particles, there may be a major turning point (in addition to small wiggling variations) around which C_{EXT} reverses its increasing/decreasing trend as the separation proceeds. (d) Even more subtle is the fact that an array's C_{EXT} does not necessarily reach its maximum or minimum value when the spheres are in contact or are well separated. The minimum/maximum value of C_{EXT} is highly dependent on the size and refractive index of the component particles as well as on their mutual separation. In one extreme case, C_{EXT} does not vary appreciably as a function of ks (figs. 3A-3I), while for another case, it changes by a factor of 7 (fig. 9B). Furthermore, no simple relationships seem to exist between maximum or minimum C_{EXT}'s and component sphere's C_{EXT}.

3.1.5 Multiple Spheres in Contact.

These multiple spheres were prepared by molding expandable polystyrene in three different-size stainless steel molds, in order to obtain at least nine identical spheres for each size. $\theta=0^{\circ}$ measurements for all of them were carried out to insure they possessed nearly the same $|S(0)|$ and $\phi(0)$ in each size group. Four or eight spheres in each group were assembled on nylon strings to form arrays of contacting square or cubic geometry, and the arrays were rotated in the incident k-H plane to obtain P, Q plots such as those shown in figures 10A-10C or in figures 11A-11C. The size parameters (x's) of the component spheres are x=3.120, 3.752 and 4.678, respectively, and the corresponding Mie scattering quantities are tabulated in table 1. Numerical data of the measured amplitude $|S(0)|$, the phase shift $\phi(0)$ and extinction efficiency Q_{EXT} are listed in table 3.

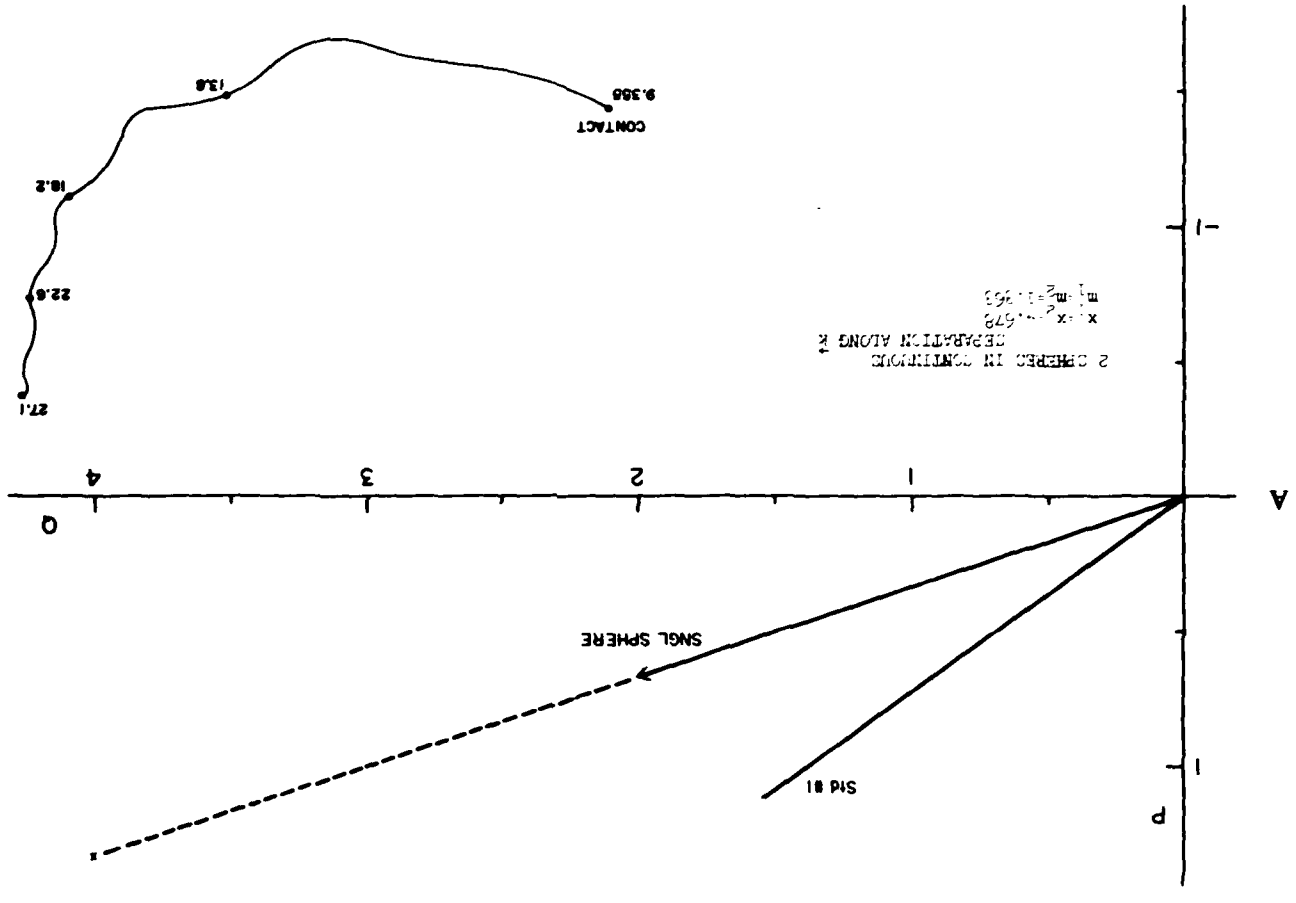

Figure 9, A. P, Q Plot of θ=0° Scattering by an Array of Two Identical Spheres in Continuous Separation along the Incident Direction. The curve is parameterized by the mutual separation (ks). See sections 3.1 and 3.1.4.

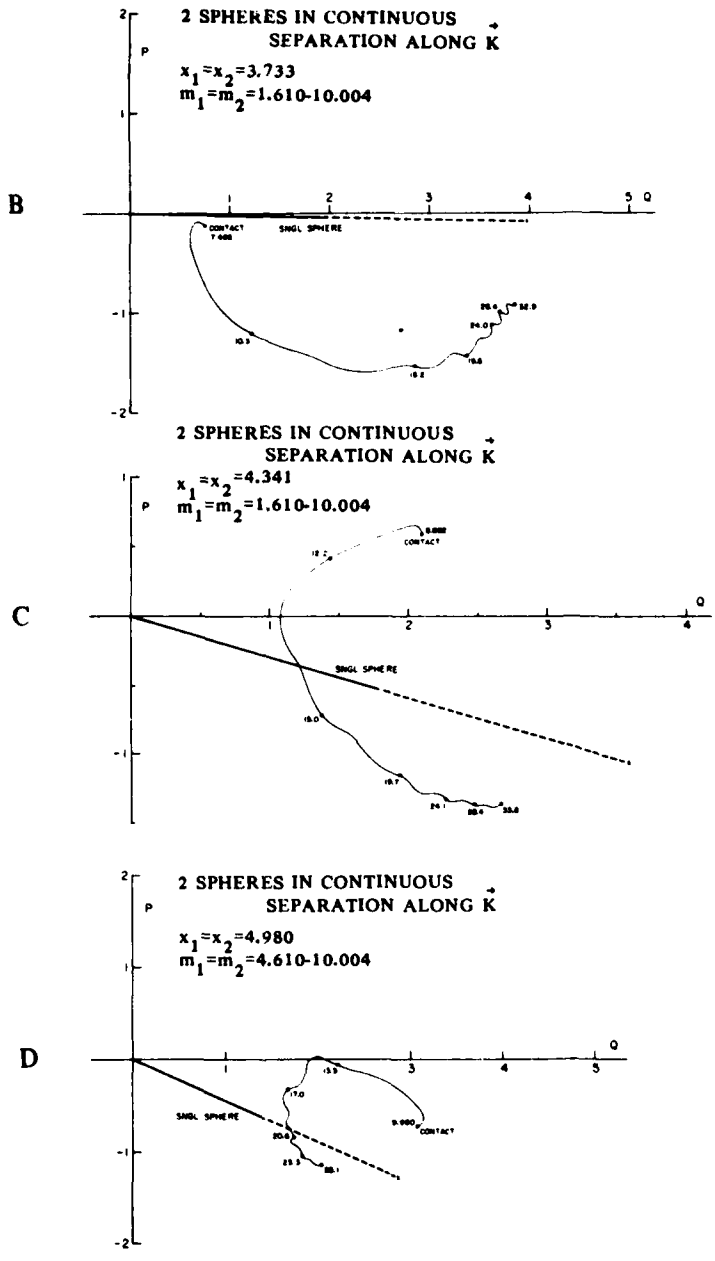

Figure 9, B to D. Same as Figure 9, A Except for the Sizes of the Arrays and Their Indexes of Refraction

Table 3. Forward Scattering Quantities of Contacting Multiple Spheres

The orientation dependence of the $\theta=0^\circ$ scattering quantities $|S(0)|$, $\phi(0)$ and Q_{EXT} for arrays of 2^n (n=1,2,3) contacting identical spheres are listed below for 3 different size groups. In each array, all component spheres are assembled on nylon strings to form a dumbbell (n=1), a square (n=2) or a cube (n=3), respectively. The array is then continuously rotated in the incident-wave k-H plane. At the orientation $\chi=0^\circ$ a straight line passing through the centers of adjoining two spheres is parallel to $\vec{k}$ but perpendicular to $\vec{H}$, while at $\chi=90^\circ$ it is perpendicular to $\vec{k}$ but parallel to $\vec{H}$.

x & m of component spheres	$N=2^n$		Orientation angle χ 0	10	20	30	40	50	60	70	80	90
	2	$\|S(0)\|$	15.96	14.79	13.78	13.08	13.08	13.44	14.13	14.86	15.07	14.97
		$\phi(0)$	77.5	75.2	71.7	64.2	55.6	48.5	42.8	41.5	42.4	43.0
		Q_{EXT}	3.20	2.94	2.69	2.42	2.22	2.07	1.97	2.02	2.09	2.10
x=3.120		$\|S(0)\|$	29.95	29.26	26.97	24.62	24.00	24.04	24.52	26.50	28.92	29.73
m=1.365	4	$\phi(0)$	81.6	81.3	81.3	81.2	77.8	77.8	79.8	80.6	80.0	80.2
		Q_{EXT}	3.04	2.97	2.74	2.50	2.41	2.41	2.48	2.68	2.92	3.01
		$\|S(0)\|$	55.72	53.57	48.60	44.59	45.01	45.17	45.17	49.31	54.12	56.08
	8	$\phi(0)$	78.6	78.1	77.5	75.1	72.7	72.7	75.5	77.7	79.0	79.5
		Q_{EXT}	2.80	2.69	2.44	2.21	2.21	2.21	2.25	2.47	2.73	2.83
		$\|S(0)\|$	21.97	20.70	19.56	19.86	20.59	21.86	23.70	24.60	24.68	24.74
	2	$\phi(0)$	109.5	103.2	90.0	77.5	67.2	59.6	56.4	55.0	55.2	55.6
		Q_{EXT}	2.94	2.86	2.78	2.76	2.70	2.68	2.80	2.86	2.88	2.90
x=3.752		$\|S(0)\|$	42.08	39.63	35.43	33.35	33.35	33.81	33.90	37.18	40.85	42.23
m=1.366	4	$\phi(0)$	106.0	103.5	98.0	92.5	91.8	91.7	93.3	99.0	104.0	105.0
		Q_{EXT}	2.87	2.74	2.49	2.37	2.37	2.40	2.40	2.61	2.82	2.90
		$\|S(0)\|$	78.17	74.39	67.45	63.86	63.80	63.23	63.36	66.51	74.89	79.93
	8	$\phi(0)$	105.8	102.7	96.0	89.7	88.0	87.7	89.4	96.0	103.4	106.7
		Q_{EXT}	2.67	2.58	2.38	2.27	2.26	2.24	2.25	2.35	2.59	2.72
		$\|S(0)\|$	27.06	28.29	31.86	33.70	36.46	39.22	41.83	43.18	43.56	43.18
	2*	$\phi(0)$	125.7	117.8	101.0	88.3	78.6	72.6	71.1	71.6	72.0	71.4
		Q_{EXT}	2.01	2.29	2.86	3.08	3.27	3.42	3.62	3.74	3.79	3.74
x=4.678		$\|S(0)\|$	49.75	47.09	46.15	44.90	44.49	44.49	44.90	46.46	47.56	50.16
m=1.363	4	$\phi(0)$	137.8	128.8	115.8	109.5	107.3	108.5	110.5	117.5	129.2	136.4
		Q_{EXT}	1.53	1.68	1.90	1.93	1.94	1.93	1.92	1.88	1.68	1.58
		$\|S(0)\|$	92.08	88.54	88.41	85.77	85.38	85.44	85.96	87.70	88.34	91.95
	8	$\phi(0)$	136.8	124.5	113.2	106.5	103.9	105.0	107.6	118.2	131.7	138.8
		Q_{EXT}	1.44	1.67	1.86	1.88	1.89	1.89	1.87	1.77	1.51	1.38

*Only for this array, the two spheres were in slight separation. The observed gap distance was 0.15 cm, which gives ks=9.65 .

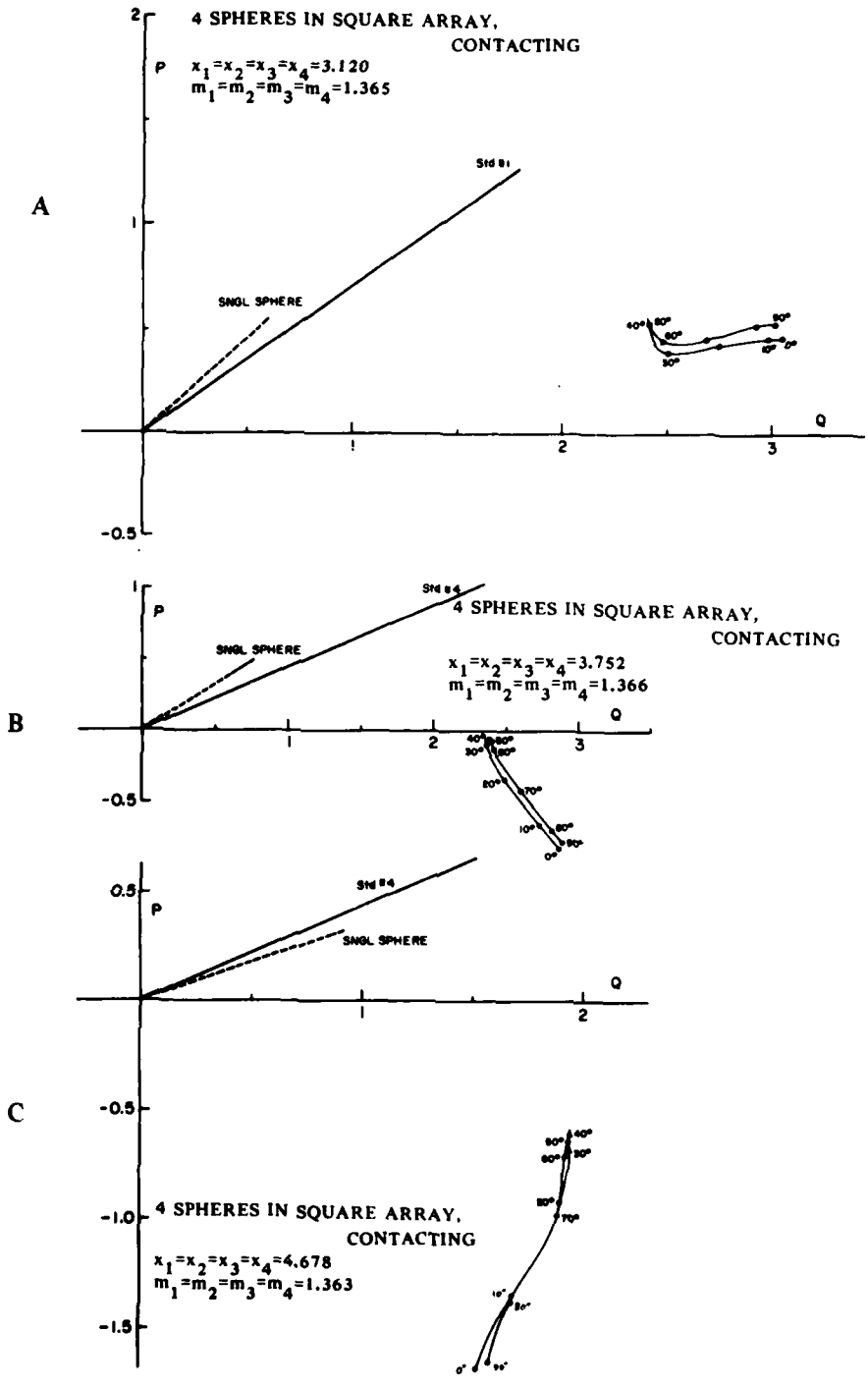

Figure 10, A to C. Three P, Q Plots, Each of Which Shows the Orientation (χ) Dependence of S(O) for a Contacting Square Array of Four Identical Spheres. At χ=0° (or 90°), one side of the square is parallel to the incident $\vec{k}$ vector, and the square is then continuously rotated in the k-H plane to generate the plot. See sections 3.1 and 3.1.5.

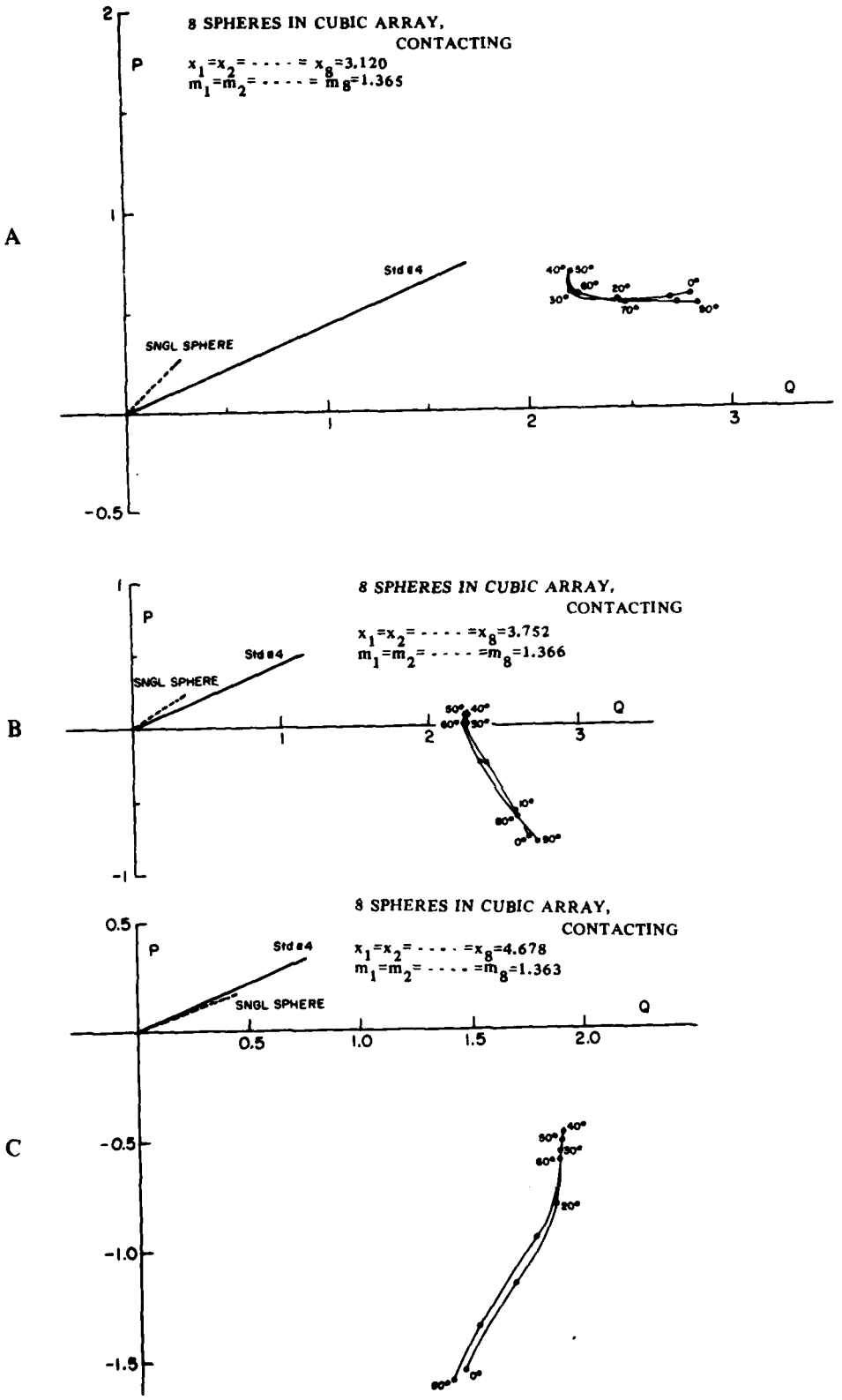

Figure 11, A to C. Same as Figure 10, A to C, Except Each Array Here Consists of Eight Contacting Identical Spheres Forming a Cube

We have previously reported a few conspicuous extinction signatures exhibited by such ensembles (Wang, 1980). Additional findings include: (a) An array of regular geometry (suggestive of atoms in a crystal lattice) shows a large variation of $|S(0)|$ and $\phi(0)$ with respect to its orientation change. Although not shown in this report, a randomly assembled array consisting of the same component spheres yields much smaller variations of $|S(0)|$ and $\phi(0)$. (b) As expected the P, Q plots appear almost symmetric about $\chi=45^{\circ}$ with respect to changes in χ. The apparent deviation from this perfect symmetry, although slight, is presently attributed to a slight variation in target parameters from one component sphere to another, along with a slight distortion of array geometry arising from the manual alignment procedure. This indicates the critical dependence of $|S(0)|$ and $\phi(0)$ on these parameters even for $\theta=0^{\circ}$ measurements. (c) Note the comparisons between figures 10A and 11A, 10B and 11B, and 10C and 11C. Each pair represents two P, Q plots of 4 and 8 identical spheres, respectively, differing only on the total number of particles in the array. The signatures are similar except that $|S(0)|$ for the 8-sphere ensemble is about twice the value of the 4-sphere ensemble. Detailed numerical data are also tabulated in table 3. This implies no appreciable interference between two 4-sphere arrays in an 8-sphere ensemble that are parallel to the k-H plane, and hence these two subarrays are scattering independently. A generalization of finding (c) may be inferred from comparisons in table 3. (d) At the particular orientation $\chi=0^{\circ}$, the 2-, 4- or 8-sphere ensembles in each size group have practically the same phase shift $\phi(0)$ but $|S(0)|$ is nearly proportional to the total number of component spheres. One is tempted to say these aggregated spheres can be split in subgroups, all parallel to the incident direction, each scattering independently of others.

3.2 Side Scattering and Angular Distribution.

Complementary to extinction measurements, observation of scattered waves from scattering angles other than $\theta=0^{\circ}$ provides an additional wealth of information about the scattering process. Because of the difficulties experienced in performing angular experiments (Wang and Greenberg, 1978), the $\theta\approx90^{\circ}$ scattering measurement was first tried before the more extensive angular distribution studies. At $\theta=90^{\circ}$, the compensation of unwanted background radiation can be neglected due to its smallness in comparison with the true scattered signal, and the target-to-wall-to-antenna secondary scattering could be reduced by placing good absorbers on that portion of wall facing the receiver antenna. The resulting measurements reveal simple-looking yet specular intensity variation as a pair of spheres was rotated in the beam. Encouraged by these results, we measured the angular distribution of $i_1(\theta)$ over the range $40^{\circ}\leq\theta\leq140^{\circ}$ in which the background level was relatively low.

3.2.1 Side Scattering ($\theta\approx90^{\circ}$).

Figures 12, A and B, show the observed intensity variation as a function of ensemble orientation χ for a pair of contacting identical spheres made of expanded polystyrene. As χ is continuously varied for the display of $i_1(\theta)$, we notice a fairly symmetrical intensity profile about $\chi = \theta/2$, which confirms the symmetry relation, Eq.(14) of Section 2.2. Disregarding the low signal-level portion, $i_1(\theta)$ goes through at least three maxima and

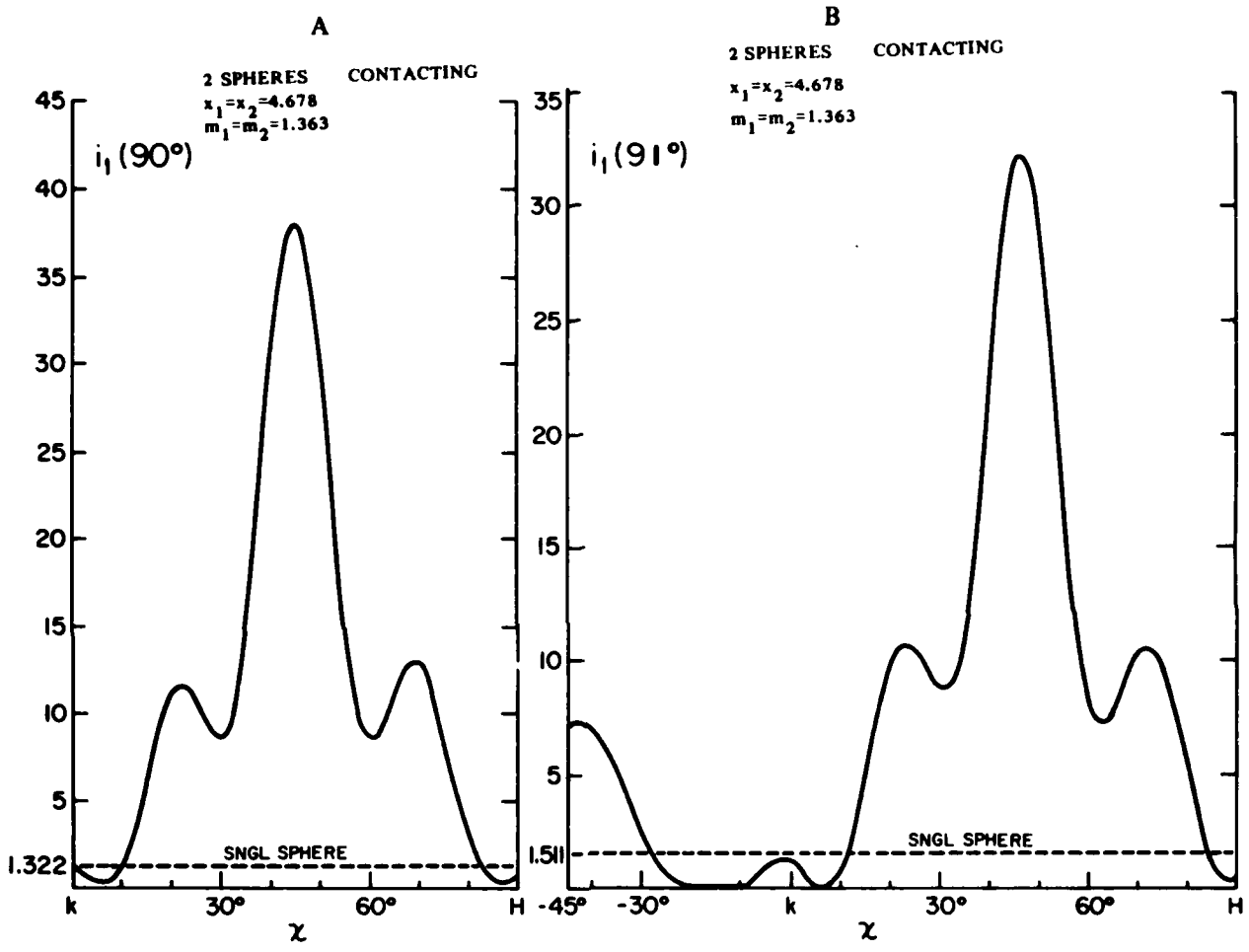

Figure 12, A and B. Scattering Intensity $i_1(\theta)$ Versus Orientation (χ) Plots for a Contacting Array of Two Identical Spheres. The array axis is parallel to the incident $\vec{k}$ vector at $\chi=0°$ (marked k) and is continuously rotated in the k-H plane in the increasing θ direction. At $\chi=90°$ (marked H) it is parellel to the $\vec{H}$ vector. See section 3.2.1. *The large resonance seen at $\chi=45°$ has neither been predicted nor experimentally observed before.* The sensitivity to scattering angle (θ) is indicated in figure 12, B where $\theta=91°$ in contrast to larger resonance shown in figure 12, A where $\theta=90°$.

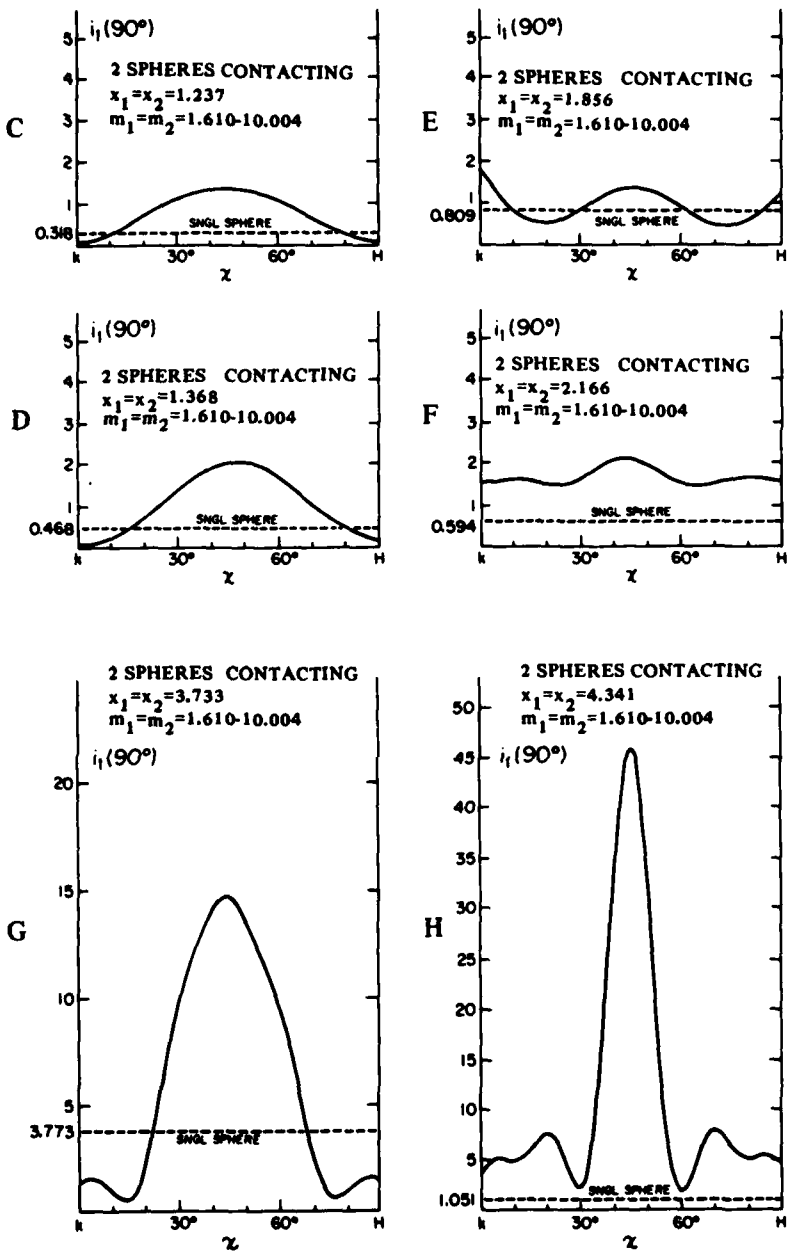

Figure 12, C to H. Same as Figure 12, A and B Except for the Index of Refraction and the Size of the Component Spheres

minima vs χ change, presumably an interference phenomenon between the dependently and independently scattered waves from the component spheres. Independently scattered waves alone could not account for the precise χ positions where these maxima/minima occurred. The most striking fact is its magnitude at $\chi=\theta/2$. In comparison with the intensity of a single sphere, as shown in each figure and in table 1, this array scatters nearly 28 times that of a component sphere at $\theta=90^{\circ}$ and 22 times at $\theta=91^{\circ}$. While the summation of *independent* scattering correctly predicts the occurrence of a maximum at this particular $\chi=\theta/2$ because of the in-phase arrivals of scattered signals from these two spheres, the maximum intensity can, at most, be 4 times that of a single sphere by this token.

Figures 12, C-H show the $i_1(90)$ vs χ plots for six pairs of 2-sphere ensembles, in the order of increasing particle size. Each pair consists of 2 contacting identical spheres of acrylic material with index of refraction m=1.610-i0.004. Each pair resembles a silicate dumbbell particle in the optical region. This series of measurements were performed to investigate in more detail the size dependence of specular scattering at $\theta=90^{\circ}$. A few conspicuous features from these plots are: (a) Similar to the previous pair of polystyrene spheres, the $i_1(90)$ vs χ profile is symmetrical about $\chi=45^{\circ}$ at which the intensity is also at a maximum, although not necessarily the maximum over the entire χ range (see fig. 12E). (b) This maximum is separated from the adjacent minimum (or maximum) by ever decreasing χ intervals as the particle grows in size - three maxima and two minima within 45° rotation from $\chi=45^{\circ}$ for a particular ensemble in figure 12H. (c) In comparison with $i_1(90)_{SNGLSPHERE}$ of a component sphere shown in each plot and in table 1, the onset of specular scattering at which $i_1(90)$ of the array is greater than $4i_1(90)_{SNGLSPHERE}$ seems to occur only for moderately larger particles (figs. 12G and 12H) and exclusively at $\chi=45^{\circ}$. For the particular ensemble shown in figure 12, H, $i_1(90)\approx 44 i_1(90)_{SNGLSPHERE}$!

3.2.2 Angular Distribution ($40^{\circ}\leq\theta\leq 140^{\circ}$).

Angular distribution data for an array of two contacting identical spheres made of expanded polystyrene is displayed in figure 13, A for two principal orientations k and H in which the array axis is parallel to the incident k and H vectors, respectively. The size of the errors associated with the smallness of the scattered intensity (except for $\theta\leq 50^{\circ}$), which is possibly mixed with uncompensated background radiation, with the uneveness of the floor (which defines the scattering plane), and with the mechanical alignment of the receiving antennas (Wang and Greenberg, 1978) are difficult to estimate; we present the data as observed.

The result for another 2-sphere ensemble is shown in figure 13, B. The two identical spheres are of acrylic material and are the same pair which showed specular reflection at $\theta=90^{\circ}$ scattering. More regularly shaped scattering lobes are observed for this particular ensemble, both for the k and H orientations. When the array axis makes an orientation angle $\chi=40^{\circ}$ from the incident direction toward the receiving direction, we see a broad scattering lobe centered around $\theta=80^{\circ}$ peaking at a large intensity. This is another confirmation of specular scattering at $\chi=\theta/2$ for this particular array. Note, however, that the standard calibration sphere used in this

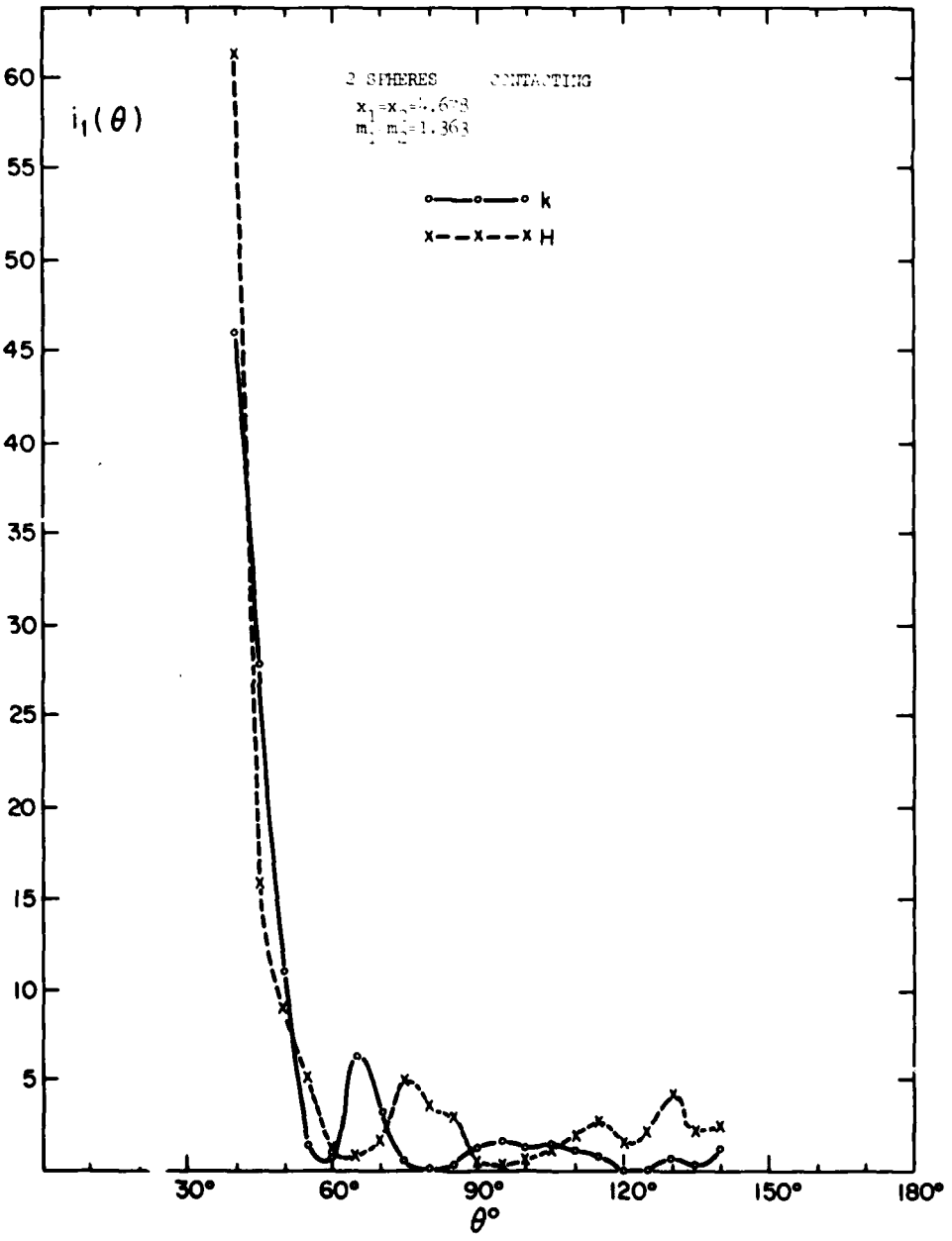

A

Figure 13, A. Angular Distribution $i_1(\theta)$ for an Array of Contacting Two Identical Spheres at Two Special Array Orientations k (array axis parallel to $\hat{k}$) and H (array axis parallel to $\hat{H}$)

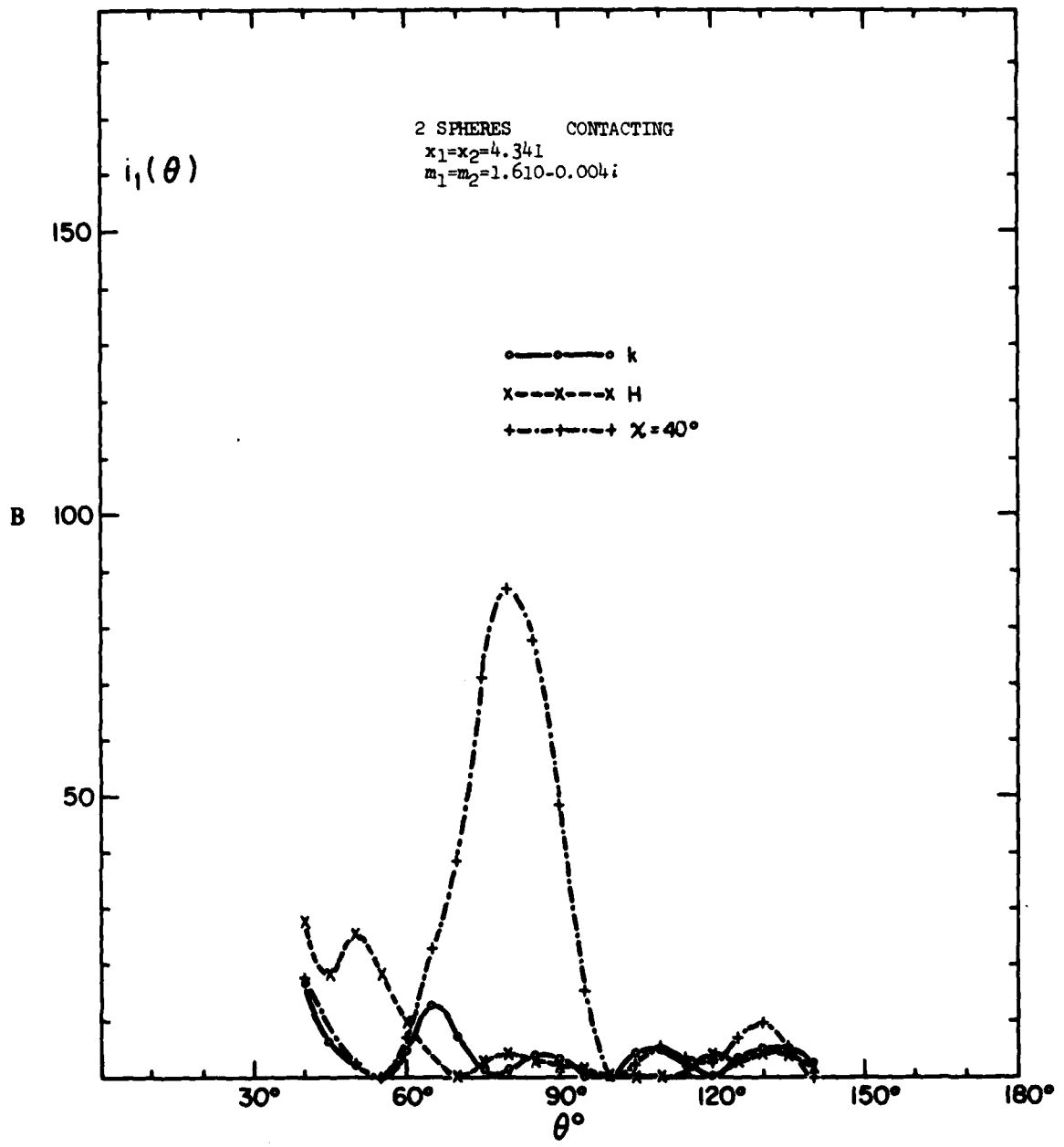

Figure 13, B. Same as Figure 13, A, Except This Array Is Made of Different Material. At the special orientation $\chi=40°$ the array axis lies in the incident k-H plane, bisecting the $\theta=0°$ and $\theta=80°$ directions

run was later found to be questionable, and hence the absolute magnitude calibrated in this figure 13, C may be in error.

4. SUMMARY REMARKS

We have reported experimental results on scattering by aggregated spheres of simple geometrical shapes. Notable findings through these microwave measurements are: (a) An ensemble of spheres of fixed geometry possesses intricate variations in its $\theta=0^{\circ}$ scattering with respect to the orientation change of the ensemble, more regularly arrayed ensembles exhibiting more pronounced variation and symmetry. (b) When the axis of two spheres is perpendicular to the incident direction, the $\theta=0^{\circ}$ scattering by the ensemble is, to a good approximation, a simple summation of independently scattering two *spheres*. To a lesser degree, this finding applies to two *arrays* aligned orthogonally to the incident direction. (c) The dependent scattering effect marks its presence at $\theta=0^{\circ}$ scattering if one of the two neighboring spheres lies within the major forward scattering lobes of the other. The angular extent of this effect decreases nonmonotonically with respect to the increasing mutual separation. (d) The P, Q plot of a contacting 2-sphere ensemble displays complex but systematic changes as the aspect angle of the array varies. The pattern is more complex for higher refracting particles than for particulates with lower indexes of refraction. A similar trend exists as the size of the component spheres increases. In particular, an interesting correlation seems to exist between an ensemble of 2 identical spheres and a prolate spheroid of 2:1 elongation possessing equal volume and refractive index. (e) The extinction of light by a pair of spheres aligned along the incident direction depends strongly on the size, index of refraction and mutual separation of component spheres. It may vary up to a factor of 7 as the separation increases, with ever slower convergence to the limit represented by the summation of extinction by component spheres. It is estimated that such a pair can be considered as independent scatterers if the separation exceeds about 10 sphere diameters. (f) Estimates of the extinction averaged over a random orientation of an ensemble of multiple spheres in this size range indicates that the ensemble obscures light more efficiently than a smooth sphere of equal total volume (Wang, 1980). (g) Certain contacting 2-sphere arrays in the resonance-size region scatter light specularly toward the direction $\underset{+}{\theta}$ when the array axis bisects this direction and the incident direction $\underset{+}{k}$.

Temporal and budgetary problems did not allow us to pursue another aspect of important measurements: repeating the measurements with incident-wave polarization changed from vertical to horizontal. Nevertheless, we believe this report contains very rare facts on a number of detailed phenomena about the dependent scattering of multiple spheres.

Acknowledgements. The authors would like to express their sincere appreciation to Dr. J. Mayo Greenberg who suggested and initiated many of the experiments reported herein. The analysis of this data was supported by the U.S. Army Research Office under contract No. DAAG29-79-C-0055.

REFERENCES

Angelakos, D.J. and Kumagai, N., 1964, *IEEE Trans. Ant. Prop.*, *AP-12*, 105.

Beard, C.I., Kays, T.H. and Twersky, V., 1962, *J. Appl. Phys.*, *33*, 2851.

Beard, C.I., Kays, T.H. and Twersky, V., 1967, *IEEE Trans. Ant. Prop.*, *AP-15*, 99.

Borghese, F., Dorti, P., Toscano, G. and Sindoni, I., 1979, *Appl. Opt.*, *18*, 116.

Bruning, J.H. and Lo, Y.T., 1969, Antenna Lab., Univ. of Illinois, Urbana, Tech. Rep. 69-5.

Bruning, J.H. and Lo, Y.T., 1971, *IEEE Trans. Ant. Prop.*, *AP-19*, 378.

Burke, J.E., Kays, T.H., Kulp, J.L. and Twersky, V., 1968, *Appl. Opt.*, *7*, 2392.

Germogenova, O.A., 1963, *Izv. Geophys. Ser.*, *648* (Akad. Nauk SSSR #4, 403).

Goyette, A. and Navon, A., 1976, *Phys. Rev. B.*, *13*, 4320.

Hansen, R.C. and Bailin, L.L., 1959, *IRE Trans. Ant. Prop.*, *7*, S458.

Hawley, S.W., Kays, T.H. and Twersky, V., 1967, *IEEE Trans. Ant. Prop.*, *AP-15*, 118.

Hongo, K., 1978, *IEEE Trans. Ant. Prop.*, *AP-26*, 748.

Kerker, M., 1969, "The Scattering of Light and Other Electromagnetic Radiation," Academic, N.Y.

Kattawar, G.W. and Humphreys, T.J., 1980, in "Light Scattering by Irregularly Shaped Particles," D.W. Schuerman, Ed., Plenum, N.Y., p. 177.

Levine, S. and Olaofe, G.O., 1968, *J. Colloid and Interface Science*, *27*, 442.

Liang, C. and Lo, Y.T., 1967, *Radio Science*, *2*, 1481.

Lind, A.C., Wang, R.T. and Greenberg, J.M., 1965, *Appl. Opt.*, *4*, 1555.

Lind, A.C., 1966, Ph.D. Thesis, Rensselaer Polytechnic Inst., Troy, N.Y.

Rhodes, D.R., 1954, *Proc. IRE*, 1408 (Sept).

Roberts, S. and von Hippel, A., 1946, *J. Appl. Phys.*, *17*, 610.

Rozenberg, V.I., 1971, (Radiotech. Electron. (Russian)) *Radio Engineering and Electronic Physics*, *16*, 394.

Silver, S., Ed., 1949, "Microwave Antenna Theory and Design," MIT Rad. Lab. Series 12, McGraw Hill, N.Y.

Silver, S., 1962, *J. Opt. Soc. America*, *52*, 131.

Sucher, M., Ed., 1963, "Handbook of Microwave Measurement," Microwave Research Inst., Brooklyn Polytech. Inst., Brooklyn, N.Y.

Trinks, W., 1935, *Ann. d. Physik*, *22*, 561.

Twersky, V., 1967, *J. Math. Phys.*, *8*, 589.

van de Hulst, H.C., 1957, "Light Scattering by Small Particles," Wiley, N.Y.

Wang, R.T., 1968, Ph.D. Thesis, Rensselaer Polytechnic Inst., Troy, N.Y.

Wang, R.T., Detenbeck, R.W., Giovane, F. and Greenberg, J.M., 1977, Final Report, NSF ATM 75-15663 (June).

Wang, R.T. and Greenberg, J.M., 1978, Final Report NASA NSG 7353 (August).

Wang, R.T., 1980, in "Light Scattering by Irregularly Shaped Particles," D.W. Schuerman, Ed., Plenum, N.Y., p. 255.

Waterman, P.C. and Truell, R., 1961, *J. Math. Phys.*, *2*, 512.

Westphal, W.B., 1954, in "Dielectric Materials and Applications," A. von Hippel, Ed., Wiley, N.Y.

Woodward, D.H., 1964, *J. Opt. Soc. America*, *54*, 1325.

DISTRIBUTION LIST 5

Names	Copies
CHEMICAL SYSTEMS LABORATORY	
ATTN: DRDAR-CLF	1
ATTN: DRDAR-CLJ-R	2
ATTN: DRDAR-CLJ-L	3
ATTN: DRDAR-CLJ-M	1
ATTN: DRDAR-CLJ-P	1
ATTN: DRDAR-CLT-E	1
ATTN: DRDAR-CLN	2
ATTN: DRDAR-CLW-C	1
ATTN: DRDAR-CLB (Mr. Vervier)	1
ATTN: DRDAR-CLB (Dr. Poziomek)	1
ATTN: DRDAR-CLB-C	1
ATTN: DRDAR-CLB-P	1
ATTN: DRDAR-CLB-PA	1
ATTN: DRDAR-CLB-PS	20
ATTN: DRDAR-CLB-PS (Display)	1
ATTN: DRDAR-CLB-PS (Pub File)	1
ATTN: DRDAR-CLB-PS (Lit File)	1
ATTN: DRDAR-CLB-R	1
ATTN: DRDAR-CLB-T	1
ATTN: DRDAR-CLB-TE	1
ATTN: DRDAR-CLY-A	1
ATTN: DRDAR-CLY-R	1
ATTN: DRDAR-CLR-I	1
ATTN: DRDAR-QAC-D	1
COPIES FOR AUTHOR(S):	
Research Division	50
ATTN: DRDAR-CLB-A (Record Set)	1
DEPARTMENT OF DEFENSE	
Defense Technical Information Center	
ATTN: DTIC-DDA-2	12
Cameron Station, Building 5	
Alexandria, VA 22314	
Director	
Defense Intelligence Agency	
ATTN: DB-4G1	1
Washington, DC 20301	
Special Agent in Charge	
ARO, 902d Military Intelligence GP	
ATTN: IAGPA-A-AN	1
Aberdeen Proving Ground, MD 21005	

Names	Copies
Commander	
SED, HQ, INSCOM	
ATTN: IRFM-SED (Mr. Joubert)	1
Fort Meade, MD 20755	
DEPARTMENT OF THE ARMY	
HQDA (DAMO-NCC)	1
WASH DC 20310	
Deputy Chief of Staff for Research, Development & Acquisition	
ATTN: DAMA-CSS-C	1
ATTN: DAMA-ARZ-D	1
Washington, DC 20310	
US Army Research and Standardization Group (Europe)	
ATTN: DRXSN-E-SC	1
Box 65, FPO New York 09510	
HQDA (DAMI-FIT)	1
WASH, DC 20310	
Commander	
DARCOM, STITEUR	
ATTN: DRXST-STI	1
Box 48, APO New York 09710	
Commander	
US Army Science & Technology Center-Far East Office	
ATTN: MAJ Borges	1
APO San Francisco 96328	
Commander	
2d Infantry Division	
ATTN: EAIDCOM	1
APO San Francisco 96224	
Commander	
5th Infantry Division (Mech)	
ATTN: Division Chemical Officer	1
Fort Polk, LA 71459	

OFFICE OF THE SURGEON GENERAL

Commander
US Army Medical Bioengineering Research
and Development Laboratory
ATTN: SGRD-UBD-AL 1
Fort Detrick, Bldg 568
Frederick, MD 21701

Headquarters
US Army Medical Research and
Development Command
ATTN: SGRD-PL 1
Fort Detrick, MD 21701

Commander
USA Biomedical Laboratory
ATTN: SGRD-UV-L 1
Aberdeen Proving Ground, MD 21010

US ARMY HEALTH SERVICE COMMAND

Superintendent
Academy of Health Sciences
US Army
ATTN: HSA-CDH 1
ATTN: HSA-IPM 1
Fort Sam Houston, TX 78234

US ARMY MATERIEL DEVELOPMENT AND
READINESS COMMAND

Commander
US Army Materiel Development and
Readiness Command
ATTN: DRCLDC 1
ATTN: DRCSF-P 1
5001 Eisenhower Ave
Alexandria, VA 22333

Project Manager Smoke/Obscurants
ATTN: DRCPM-SMK 1
Aberdeen Proving Ground, MD 21005

Commander
US Army Foreign Science & Technology Center
ATTN: DRXST-MT3 1
220 Seventh St., NE
Charlottesville, VA 22901

Director
US Army Materiel Systems Analysis Activity
ATTN: DRXSY-MP 1
ATTN: DRXSY-TN (Mr. Metz) 2
Aberdeen Proving Ground, MD 21005

Commander
US Army Missile Command
Redstone Scientific Information Center
ATTN: DRSMI-RPR (Documents) 1
Redstone Arsenal, AL 35809

Director
DARCOM Field Safety Activity
ATTN: DRXOS-C 1
Charlestown, IN 47111

Commander
US Army Natick Research and
Development Command
ATTN: DRDNA-VR 1
ATTN: DRDNA-VT 1
Natick, MA 01760

US ARMY ARMAMENT RESEARCH AND
DEVELOPMENT COMMAND

Commander
US Army Armament Research and
Development Command
ATTN: DRDAR-LCA-L 1
ATTN: DRDAR-LCE 1
ATTN: DRDAR-LCE-C 1
ATTN: DRDAR-LCU 1
ATTN: DRDAR-LCU-CE 1
ATTN: DRDAR-PMA (G.R. Sacco) 1
ATTN: DRDAR-SCA-W 1
ATTN: DRDAR-TSS 5
ATTN: DRCPM-CAWS-AM 1
ATTN: DRCPM-CAWS-SI 1
Dover, NJ 07801

Director
Ballistic Research Laboratory
ARRADCOM
ATTN: DRDAR-TSB-S 1
Aberdeen Proving Ground, MD 21005

US ARMY ARMAMENT MATERIEL READINESS COMMAND

Commander
US Army Armament Materiel
Readiness Command
ATTN: DRSAR-ASN 1
ATTN: DRSAR-PDM 1
ATTN: DRSAR-SF 1
Rock Island, IL 61299

Commander
US Army Dugway Proving Ground
ATTN: Technical Library Docu Sect 1
Dugway, UT 84022

US ARMY TRAINING & DOCTRINE COMMAND

Commandant
US Army Infantry School
ATTN: NBC Division 1
Fort Benning, GA 31905

Commandant
USAMP&CS/TC&FM
ATTN: ATZN-CM-CDM 1
Fort McClellan, AL 36205

Commander
US Army Infantry Center
ATTN: ATSH-CD-MS-C 1
Fort Benning, GA 31905

Commander
US Army Infantry Center
Directorate of Plans & Training
ATTN: ATZB-DPT-PO-NBC 1
Fort Benning, GA 31905

Commander
USA Training and Doctrine Command
ATTN: ATCD-Z 1
Fort Monroe, VA 23651

Commander
USA Combined Arms Center and
Fort Leavenworth
ATTN: ATZL-CA-COG 1
ATTN: ATZL-CAM-IM 1
Fort Leavenworth, KS 66027

Commander
US Army TRADOC System Analysis Activity
ATTN: ATAA-SL 1
White Sands Missile Range, NM 88002

US ARMY TEST & EVALUATION COMMAND

Commander
US Army Test & Evaluation Command
ATTN: DRSTE-CM-F 1
ATTN: DRSTE-CT-T 1
Aberdeen Proving Ground, MD 21005

DEPARTMENT OF THE NAVY

Commander
Naval Explosive Ordnance Disposal Facility
ATTN: Army Chemical Officer (Code AC-3) 1
Indian Head, MD 20640

Commander
Naval Weapons Center
ATTN: Technical Library (Code 343) 1
China Lake, CA 93555

Commander Officer
Naval Weapons Support Center
ATTN: Code 5042 (Dr. B.E. Douda) 1
Crane, IN 47522

US MARINE CORPS

Director, Development Center
Marine Corps Development and
Education Command
ATTN: Fire Power Division 1
Quantico, VA 22134

DEPARTMENT OF THE AIR FORCE

HQ Foreign Technology Division (AFSC)
ATTN: TQTR 1
Wright-Patterson AFB, OH 45433

HQ AFLC/LOWMM 1
Wright-Patterson AFB, OH 45433

OUTSIDE AGENCIES

Battelle, Columbus Laboratories
ATTN: TACTEC 1
505 King Avenue
Columbus, OH 43201

Toxicology Information Center, WG 1008
National Research Council 1
2101 Constitution Ave., NW
Washington, DC 20418


DA
FIL